The Effect of Eurasian Snow Cover on Regional and Global Climate Variations

T. P. BARNETT

Climate Research Group, Scripps Institution of Oceanography, La Jolla, California

L. DÜMENIL, U. SCHLESE AND E. ROECKNER

Meteorologisches Institut, University of Hamburg, Hamburg, FRG

M. LATIF

Max-Planck-Institut für Meteorologie, Hamburg, FRG

(Manuscript received 30 March 1988, in final form 28 September 1988)

ABSTRACT

The sensitivity of the global climate system to interannual variability of the Eurasian snow cover has been investigated with numerical models. It was found that heavier than normal Eurasian snow cover in spring leads to a "poor" monsoon over Southeast Asia thereby verifying an idea over 100 years old. The poor monsoon was characterized by reduced rainfall over India and Burma, reduced wind stress over the Indian Ocean, lower than normal temperatures on the Asian land mass and in the overlying atmospheric column, reduced tropical jet, increased soil moisture, and other features associated with poor monsoons. Lighter than normal snow cover led to a "good" monsoon with atmospheric anomalies like those described above but of opposite sign. Remote responses from the snow field perturbation include readjustment of the Northern Hemispheric mass field in midlatitude, an equatorially symmetric response of the tropical geopotential height and temperature field and weak, but significant, perturbations in the surface wind stress and heat flux in the tropical Pacific.

The physics responsible for the regional response involves all elements of both the surface heat budget and heat budget of the full atmospheric column. In essence, the snow, soil and atmospheric moisture all act to keep the land and overlying atmospheric column colder than normal during a heavy snow simulation thus reducing the land–ocean temperature contrast needed to initiate the monsoon. The remote responses are driven by heating anomalies associated with both large scale air–sea interactions and precipitation events.

The model winds from the heavy snow experiment were used to drive an ocean model. The SST field in that model developed a weak El Niño in the equatorial Pacific. A coupled ocean–atmosphere model simulation perturbed only by anomalous Eurasian snow cover was also run and it developed a much stronger El Niño in the Pacific. The coupled system clearly amplified the wind stress anomaly associated with the poor monsoon. These results show the important role of an evolving (not specified) sea surface temperature in numerical experiments and the real climate system. Our general results also demonstrate the importance of land processes in global climate dynamics and their possible role as one of the factors that could trigger ENSO events.

1. Introduction

It has been speculated for over a century that the varying extent and thickness of the Eurasian snow cover exerted some degree of control over both regional and, perhaps, global climate change. Blanford (1884) was one of the first to suggest the summer monsoon over India and Burma might be influenced by the spring snow cover on the Himalayas. He further guessed that such a relation, if thermally driven, might involve "major portions of the Asiatic continent rather than merely a relatively small portion of its mountain axis". These suggestions, or variants thereof, have been put forth by other investigators in the intervening period. Most recently, Barnett (1985a) invoked Asian snow cover and the associated hydrological–atmospheric interactions to explain a key set of teleconnections associated with global-scale sea level pressure signals. Yasunari (1987) offered evidence to further substantiate this latter suggestion. The purpose of this paper is to demonstrate that the speculation of the last 100+ years is strongly supported by theory, numerical model results, and observations. In essence, we show that the old ideas are valid although the physics responsible for the pertinent relationships are more complicated than previously guessed.

The physical scenario that supports the above speculation is appealing. With the advent of spring, the Asian landmass warms until it and the air above it are warmer than the surrounding ocean. The land–sea temperature contrast then initiates the surface circulation from sea to land in the familiar summer mon-

Corresponding author address: Dr. Barnett, Scripps Institution of Oceanography, USCD-Mail Code A-024, La Jolla, CA 92093.

soon pattern. Interaction of this flow with the Southeast Asian highlands results in heavy precipitation and subsequent release of latent heat. The combination of land–sea temperature contrast and latent heat release are thought to drive the monsoon system (e.g. Ramage 1971; Hastenrath 1985; He 1987; Fein and Stevens 1987). With this simple view of the summer monsoon, it is clear that a diminution or delay of the normal warming of the land surface would give rise to a delayed or weakened monsoon circulation. The albedo associated with the snow cover would lessen the amount of solar radiation absorbed by the ground. An unusually heavy snow cover would keep the ground cold longer than normal since the heat of fusion required to melt the snow would not be available to warm the surface. Both effects would keep the landmass colder than normal. The effect of the melt water from the snow would also increase the soil moisture and the groundwater reservoir would be increased. The subsequent evaporation would also keep the ground cool. This combination of physical ideas could, if operative, affect the response envisioned above.

The actual evidence available to support the regional hypothesis, i.e., the coupling between Asian snow cover and subsequent summer monsoon, is meager. Blanford (1884) and Walker (1910) were apparently the first to correlate some measure of snow extent with Indian rainfall. More recently, Hahn and Shukla (1976) correlated satellite-derived snow cover over Southeast Asia with subsequent changes in monsoon precipitation. They found a significant correlation from an extremely limited and imperfect dataset. Dey and Bhanu Kumar (1982, 1983) and Dickson (1984) performed similar analysis with slightly longer and improved datasets and reproduced the same results. However, all of these calculations are sensitive to uncertainties in the snow data, which was derived from satellite observations (cf. Kukla and Robinson 1981; Matson and Wiesnet 1981; Ropelewski et al. 1984). In any event, these studies all concentrated on areal coverage of the snow field; not its mass field (snow depth). Thus the empirical studies while supportive of the snow cover–monsoon connection are far from conclusive. Similar studies using data from the United States by Namias (1962, 1985) and Walsh et al. (1985) also suggest the contemporaneous relationship between snow amount and temperatures at least in the lower troposphere.

The role of the monsoon in larger scale global climate variations has only begun to be studied. What evidence exists seems to suggest that there is a reasonably strong relation between El Niño/Southern Oscillation (ENSO) events and monsoon variations, with the warm phase of these events being typified by lower than normal precipitation in Southeast Asia. Such results were found empirically by Weare (1979), Angell (1981) and Mooley and Parthasarathy (1983), among others. All suggest that positive equatorial sea surface temperatures (SST) anomalies in the central and eastern Pacific tend to follow a poor (summer) monsoon over Asia. Tanaka (1980) came to a similar conclusion regarding the interrelation of ENSO events, the tropical easterly jet, and the monsoon. In contrast, Rasmusson and Carpenter (1983) use a composite analysis to suggest that the changes in the sea surface temperature off the coast of South America, which they found normally to peak in April and May, precede the monsoon season by a month or two. The sign of the correlation they discuss is as found by the previous authors. However, the timing of maximum SST off South America is subjective, poorly defined and not well related to the seasonal cycle in these composites so lead/lag relations are hard to discern. However, a rigorous study of the lead/lag relations between monsoon rainfall and eastern Pacific SST using 80 years of data clearly shows SST changes to be coincident with or lag summer monsoon rainfall (e.g. Khandekar and Neralla 1984). Elliott and Angel (1987) show the same lag relationship and also suggest it includes the Southern Oscillation as well (cf. Wu and Hastenrath 1986). In summary, there is an apparent link between the warm extremes of ENSO events and poor summer monsoons with many quantitative analyses suggesting monsoon variations occur with or foreshadow some, but not all, of the main ENSO signals.

There are additional sets of impressive diagnostic studies that suggest there should be a close relation between the monsoon circulation over Southern Asia and other prominent climatic features in the tropics. The studies of Johnson et al. (1985), Wei et al. (1983) and the pioneering effort of Krishnamurti (1971) and others cited above all show the region of Southeast Asia to be a major source of mass and energy for the general circulation during the northern summer. It follows that any fluctuations of mass and energy export from this critical region, i.e., monsoon fluctuations, should have repercussions in other parts of the globe (cf. Lau and Li 1984, for a descriptive example).

There is some indirect theoretical support for the snow–monsoon interaction. For instance, Roads (1981) showed that the anomalous snow cover on the east side of the North American continent could generate the type of near surface pressure systems suggested by Namias (1962, 1985) via a snow–albedo feedback mechanism. In a more complex set of experiments, Yeh et al. (1983) found that removal of the snow cover can affect the overlying model atmosphere in a number of ways. Removal of the snow changes the surface albedo and increases absorption of incoming solar energy. This is similar to the type of feedback described by Roads. More importantly, they found that the snow melt could affect the soil moisture and subsequent evaporation. In their idealized numerical experiments, these changes had an impact on the temperature of the atmosphere from the surface to the upper troposphere. Finally, Kutzbach (1981), simulating the monsoon climate during the early Holocene, found that an increase in

solar radiation led to a stronger warming of the Asian landmass and a strengthened summer monsoon. A final cautionary remark should be noted based on the work of Robock (1983) who found the role of sea ice to be more important in a simple climate model than snow–albedo feedback.

In the following sections of this paper, we describe the characteristics of the numerical model used to conduct the snow cover sensitivity tests and then investigate the ability of the model to reproduce the major features of the summer monsoon over Southeast Asia. We next describe an experiment to determine the role of albedo in the atmospheric response to anomalous snow cover. The following section investigates the effect of anomalous snow depth in influencing subsequent atmospheric properties on both a regional and global scale. It will be shown that the snowmass (depth) appears to be the key climatological variable in effecting an atmospheric response. The physics associated with this complex interaction are discussed next and followed by a numerical demonstration that snow-induced perturbations in the Pacific tradewind could serve as a trigger for El Niño events.

2. Description of the GCM and significance tests

a. Model

The general circulation model used in this set of low resolution climate integrations is a derivative of the ECMWF (European Centre for Medium Range Weather Forecasts) spectral medium-range forecasting model (Fischer 1987). T21 denotes the spectral model version with triangular truncation of the spherical harmonic representation of model fields at wavenumber 21. Nonlinear terms and physical processes are evaluated at grid points of an almost regular "Gaussian" grid providing a resolution of 5.625° in latitude and longitude. Discretization in the vertical is done employing a vertical finite difference scheme in a hybrid coordinate system. The T21 model uses 16 levels combining a sigma-coordinate near the surface with a pressure coordinate in the stratosphere (Simmons and Burridge 1981). The uppermost level is at 25 hPa. The temporal finite difference scheme is semi-implicit with a timestep of 2700 seconds.

Contrary to the "envelope" orography (Wallace et al. 1983) used in higher resolution versions of the model, the T21 model employs a spectrally fitted orography representation based on mean values for the specified model grid derived from a high resolution dataset.

The parameterization of physical processes in the model comprises radiation, cloud cover, large-scale condensation and deep convection schemes (Kuo 1974), turbulent vertical diffusion and three layer diffusion of heat and moisture in the ground. There is no diurnal cycle of radiation. The deep convection and large-scale condensation schemes, respectively, account for precipitation as rain or snow with snow cover being accumulated at the surface.

At land points, surface temperature as the lower boundary condition is a prognostic variable derived from a surface heat balance equation and diffusion through the soil. The diffusion of heat and moisture in the ground is based on values representative of three layers in the soil with depths of 7.2 cm for the uppermost layer and 43.2 cm for the two layers below such that the system may respond to a daily cycle as well as longer term forcing. For the lowest layer in the ground, climatological temperature and moisture content are prescribed by updating the fields with climatology every fourth day during a seasonal cycle integration. The soil characteristics are taken as equal for all land areas (product of density and heat capacity $\rho_g C_g = 2.4 \times 10^6$ J m^{-3} K^{-1}, heat diffusivity $\kappa = 7.5 \times 10^{-7}$ m^2 s^{-1}). The albedo of the surface is prescribed according to geographic conditions over the globe except that it is a function of local snow conditions. An albedo of 0.60 is taken for full snow coverage although eventually a more sophisticated representation may be required (Robock 1983).

Atmospheric forcing of the surface temperature (T_S) is given by the heat budget at the surface due to the sum of solar and thermal radiative fluxes, sensible and latent heat fluxes. Additionally, T_S is modified by the melting of snow. In the equation of surface wetness (the amount of water present in the top soil layer), precipitation, surface moisture fluxes in snow free areas or snow melt water, and diffusion in the soil are considered. Runoff occurs for layer moisture contents larger than 0.02 m. At sea-points, sea surface temperatures are prescribed according to climatology. They are updated every fourth day. The model distinguishes between open water and sea ice. The underlying sea ice mask is defined if the climatological sea surface temperatures are below −2°C. Any variation in sea ice is associated with a change of roughness length z_0 and surface albedo. Persistent ice cover over land is represented by large snow heights with corresponding surface albedo.

b. Significance tests

Results to be presented in subsequent sections will generally contrast the differences between monthly averages of a control (C) and perturbation (P) experiment. It will often be convenient to express the results in normalized form

$$\Delta = \frac{\mathrm{P} - \mathrm{C}}{\sigma}$$

where σ is the monthly standard deviation computed from the 10-year control run. The measure Δ is closely related to a t-statistic often used to test model significance (e.g., Chervin and Schneider 1976). However, the field significance of such a statistic is a serious

problem (cf. Livezey and Chen 1983). In this paper, we used the PPP significance tests described by Preisendorfer and Barnett (1983) to resolve questions of significance since this test automatically solves problems of field significance and has high statistical power. In general, the PPP test is more rigorous than a consideration of individual t-statistics. Thus, while we show many of the results graphically in terms of Δ, significance statements are made based on the PPP test. We will not belabor the significance issue further here or later in the text, other than to say the results to be shown have met a demanding nonparametric significance criteria that clearly shows when the P experiments differ from the C run with confidence equal or exceeding 0.95 unless otherwise noted.

3. Monsoon simulation

The purpose of this section is to provide a brief overview of the model's ability to simulate the snowfield and summer monsoon over Eurasia. Prior studies of this type, more extensive than reported here, have yielded encouraging results (cf. Fischer 1987). Here we concentrate on showing examples of averages of the 10-year control run for climatic fields to be discussed in later sections. All in all, the model does a surprisingly good job of reproducing the main features of the monsoon and other important Asian climate fields. It must be remembered here and in the rest of the paper that it is the large scale features of the entire Asian monsoon that we shall be discussing, not the structure of its subelements, e.g. the Indian monsoon.

A key monsoon variable is precipitation. The distribution of model simulated precipitation in June is typical of other summer monsoon months and is compared with observations of Jaeger (1976) in Fig. 1. The largest area of intense precipitation occurs in both model and observations over the Bay of Bengal–Burma region with secondary maxima along the equator between New Guinea and the dateline, over the Philippines and in northeast China. Another maximum on the west coast of India in the vicinity of the Ghat Mountains is not well simulated, but the feature is related to orography which is smaller than the model's spatial resolution so the failure is not surprising. The observed 10 cm contour of precipitation in the Western Pacific is well reproduced by the model. The same cannot be said for the 10 cm contour in the western Indian Ocean; an area where the data is sparse. However, the overall impression is that this relatively coarse resolution model is doing a rather good quantitative job of reproducing the large-scale space and time distribution of precipitation over the region of interest.

The distribution and depths of snow in the control simulation are compared in Fig. 2 with observations of the snow depth field over Eurasia for the critical months of April and May. The observations, courtesy of the U.S. Air Force ETAC, were derived largely from

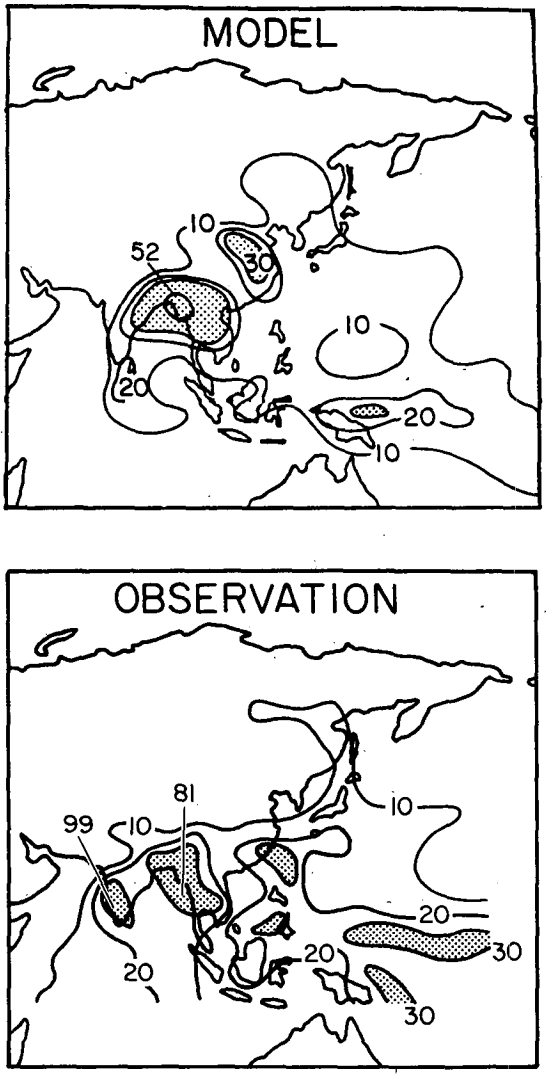

FIG. 1. Comparison between the June precipitation climatology from the model and from the observations of Jaeger (1976). Regions with more than 30 cm precipitation during the month are stippled (units are centimeters). Regions with less than 10 cm precipitation are omitted.

station data and are therefore least reliable in the central and southeastern parts of Asia. The ETAC climatology compares favorably with that of Kopanev and Lipovaskaya (1978) and Schutz and Bregman (1987), although the snow depths in the latter set tend to be larger than shown in Fig. 2. It is clear that the snow depths produced by the model are reasonably close to the observations[1] over most of Asia, although there is a distinct tendency for the model to have more snow than observed. The model snow line for selected

[1] Observed snow depth was converted to equivalent water content for comparison with the model. The snow density was taken to be 0.3 g cm^{-3}, a conservatively low value over much of Asia for the late spring season (Bilello 1984; Rikhter 1954).

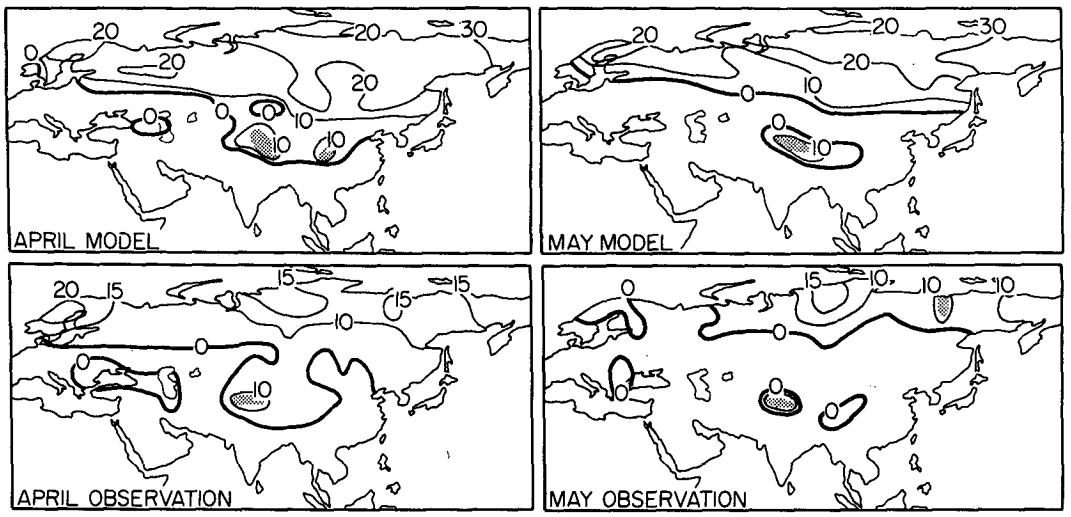

FIG. 2. The comparison of the snow distribution and depth given by the model's climatology with observations. The contours estimate snow depth in centimeters of equivalent water. The heavy solid line indicates the approximate position of the snow line. The stippled areas represent large snow accumulations associated with the Himalayas, etc.

months was also compared with the ETAC and Soviet climatologies and with the monthly snowlines position obtained from satellite data (cf. Matson and Wiesnet 1981). We found that the model snowline was generally located in a more southerly position than given by the satellite or station data. The results suggested the model's snow line retreats with about a one month lag relative to the observed snow line. Inspection of each year of the 10-year control run also showed the model snow line had very little year-to-year variability for a specific month. In summary, the model's ability to simulate the amount and distribution of snow over Eurasia, while in need of some improvement, is better than we would have guessed and seems adequate for the numerical experiments to be reported below.

The distributions of model and observed sea level pressure in June are shown in Fig. 3. The spatial development of the model low over Southeast Asia is good although the magnitude is too low by up to 8 mb. This underestimation seems to be a general feature of the model's global SLP field. The spatial features of the SLP field in other parts of the globe plus other pressure surfaces (up to 200 mb) are equally well reproduced qualitatively, but again tend to be lower than observed. The temporal evolution of these features over Eurasia with season (not shown) is also in agreement with observations, cf. Tanaka (1980). A more detailed analysis of the model's ability to reproduce the global geopotential field is given in Fischer (1987).

The wind field developments that accompany the above changes in the mass field are similar to those found in the observations. For instance, the onset of the monsoon finds the development and strengthening of a low latitude easterly jet at 200 mb just as described by Tanaka (1980). The maximum speed of the model jet (-27 m s^{-1}) compares fortuitously well with the long term mean values given by Tanaka (-24 m s^{-1}). The surface (10 m) wind field over the Indian Ocean agrees well with long term means from ship observations as shown in Fig. 4. In fact, a detailed comparison between the near-surface winds from T21 and ship observations shows the model does a surprisingly good job of reproducing the observations throughout the tropics although it does have several important shortcomings (Graham et al. 1988).

In summary, the T21 model does a creditable, qual-

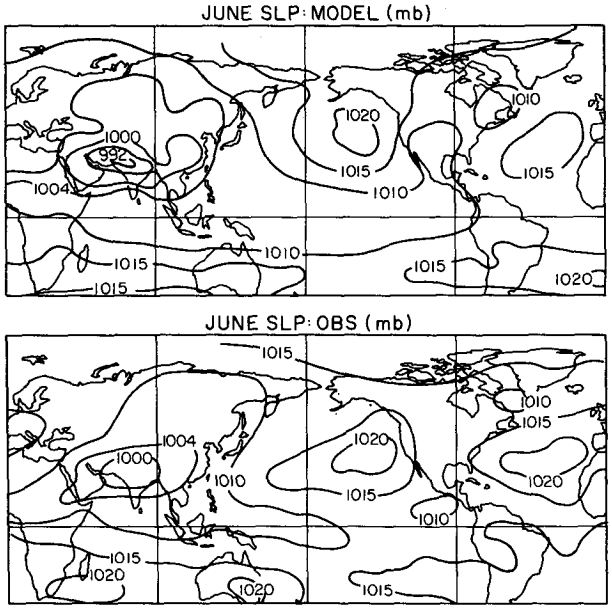

FIG. 3. Comparison of the average June sea level pressure field from the model's 10-year control run with that for a long term June average of observations.

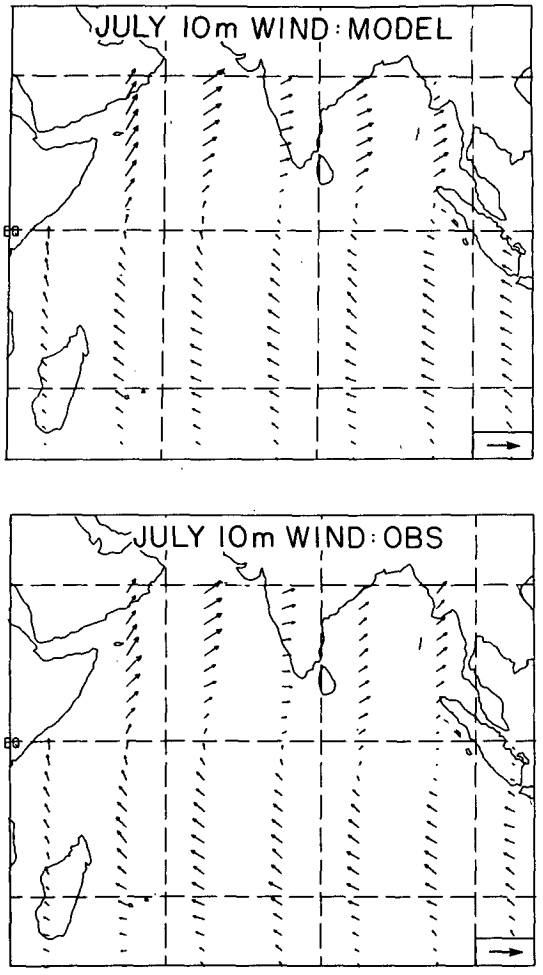

FIG. 4. Comparison of averaged control run July wind velocity with the long term mean obtained from ship reports. The winds are typical of 10-meter anemometer height. The large arrow in the lower right corner of each panel corresponds to an eastward directed wind of 20 m s^{-1}. The model winds have been projected onto the 2° × 10° grid of the observation set. This illustration is courtesy of N. Graham.

itative job of reproducing key climatic features associated with the Asian Monsoon. Many of the fields (e.g. winds, precipitation), are also accounted for with good qualitative accuracy. The snow field simulations in the model are realistic with respect to depth but the snow line tends to retreat somewhat more slowly than observed. Considering the model's strengths and weaknesses, it appears quite capable of providing a reliable base for monsoon perturbation experiments.

4. Hypothesis I: Albedo feedback

The basic idea to be tested was that the albedo associated with realistic distributions of snow cover over Eurasia could have an appreciable effect on the subsequent monsoon development. The basic problems in this experiment were to obtain realistic estimates of extreme snow coverage situations and to isolate the albedo mechanism from other competing physical processes (e.g. evaporation) in the simulations.

a. Experimental setup

Two experiments were run to test the albedo feedback idea. In the first, denoted A78, the snow cover was prescribed at each time step to correspond to the snow line observed by satellite during the first half of 1978. This represents a realistic case where the areal extent of snow coverage is the maximum observed during the 13-year satellite dataset (cf. Matson and Wiesnet 1981). A second case, denoted A70, was run using the minimum observed snow coverage during the 13-year set and that occurred in 1970. There was a 500–2000 km meridional separation in snow lines between these two extremes in several spring months over Asia (cf. Fig. 5). Also note the full continental dimension of the snow line position anomaly. In both cases, the snow depth, where prescribed, was set to 2 cm of equivalent water which represented total coverage for the grid area thus fixing the surface albedo to be that associated with total snow cover. Using this same value in the two simulations also helped to minimize any soil moisture difference between experiments. This prescription of snow cover according to

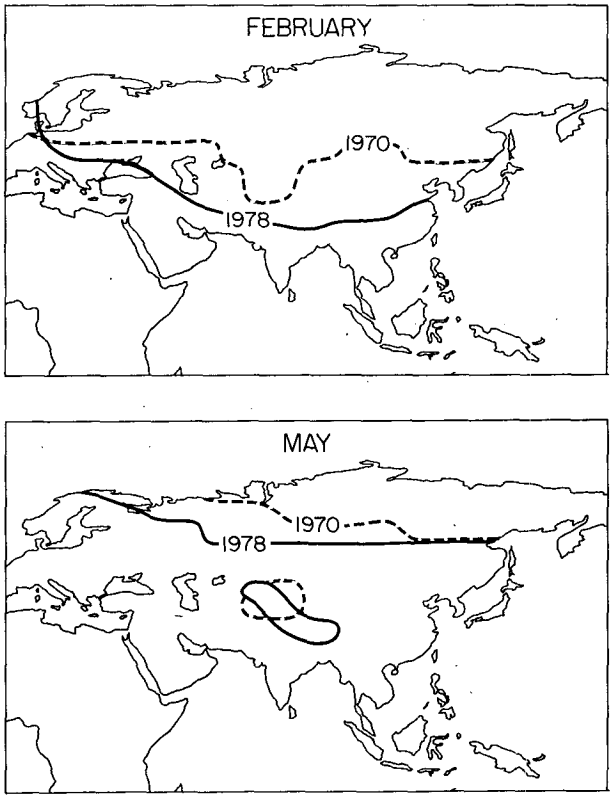

FIG. 5. Snowline position from satellite observations for February and May 1970 and 1978.

observations was only applied in the Eurasian region of the model domain. In all other regions of the globe the snow cover was defined for each month by the 10-year mean value of a control integration.

The parameterization of the hydrological cycle was left unaltered in terms of atmospheric thermodynamics. Precipitation was produced both as rain and snow, but model computed snowfall did not accumulate at the surface. All processes associated with snow melt and evaporation from snow covered surfaces were suppressed to isolate any albedo effects from other hydrological processes. Finally, all other required boundary conditions were set at the same seasonally varying values as used in the control run.

The integrations were started from a 1 January initial condition taken from the third year of the control run. The calculations were carried through to the end of June by which time the snow had for all practical purposes vanished, except right on the Himalayas. Truncation of the experiment in June was dictated by the results discussed below.

b. *Results*

The winter months of the model integrations with altered snow line showed small, generally insignificant anomalies relative to the control run. However, as the zenith angle of the sun rose with the approach of spring the anomalies became larger and by May were statistically significant in the geopotential height field. However, the significant differences between the A78 and A70 experiments were confined to the immediate locale of the snowline anomaly. Also, the significant signals appeared in only a few of the fields investigated. No substantial signals could be found in the SLP, surface wind, or precipitation fields. Further, all significant signals vanished with the disappearance of the snow. Thus, the model's climate system, although partially perturbed, showed no memory and no tendency to attain climate states that differed significantly between A78 and A70.

In summary, we conclude that the albedo effect, associated with the anomalous spatial distribution of snow, cannot, by itself, have a sustained impact on subsequent monsoon development. The model results suggest that we reject Hypothesis I.

5. Hypothesis II: Hydrological feedback

The basic idea to be tested in this set of experiments was that variations in the snow *depth* and its subsequent melting, evaporation, and influence on the soil hydrology would cause an atmospheric response which could effect monsoon development. Our major modeling problem was to alter snow depth without dramatically affecting the energy balance in the model. The results expected a priori were that a deeper than normal Eurasian snow cover would lead to a "poor" monsoon while a shallower than normal snow cover would lead to a "good" monsoon. By "poor" monsoon we mean a reduction in precipitation over Southeast Asia, increased surface pressure, reduction in both the surface winds and tropical easterly jet and colder than normal atmospheric temperature over Asia (cf. Hastenrath 1985; Fein and Stevens 1987). A "good" monsoon is taken to be the converse of a "poor" monsoon.

a. *Experimental setup*

In this experimental series we wished to change the snow depth but leave the model otherwise free to carry through its hydrological cycle. This was a difficult task since we are dealing with an interactive variable, not a passive one (like in SST sensitivity experiments). The way we accomplished this was to simply double or halve the snowfall rate given by the model's condensation schemes without implications for the atmospheric heat and moisture balance at the time it falls. At the surface, snow depth is accumulated at twice (or one half) the normal rate and therefore a larger (smaller) amount of snow is available for melting and evaporation processes at the later stages of the simulation. This approach is reasonably consistent from an energetics point of view; a situation that repeating the Hypothesis I experiment with more or less snow would not satisfy. This procedure is not without its drawbacks. For instance, over how large an area should snowfall be increased/decreased? We applied the altered snowfall rates applied only to the Eurasian continent since the observed snowline variations (Fig. 5) suggest a continental scale is appropriate to the snow depth anomaly field. In fact, this may be an over estimation but there is little evidence to guide us otherwise. All other aspects of the hydrological cycle were handled as in the control runs, as was the specification of all other seasonal forcing terms.

Four sets of integrations were initialized with 1 January data from four different years of the control run. We designated the group of four doubled snowfall rate experiments by "D" and the group of four halved-rate experiments by "H". This provided four realizations of D and four of H conditions—an adequate sample for the nonparametric significance tests mentioned in section 2. Results from these groups of simulations were averaged together and compared with the control. Thus the results below will represent, say, the average of the four D experiments, referred to simply as D, minus the mean control; the difference typically being normalized by the standard deviation of the control run (cf. section 2b).

Perhaps the most critical aspect of the experiments is the size of the induced snow anomalies. The variability between the D (H) experiments and the control should be comparable to the variations observed in nature. We investigated the relative size of the model anomalies in several ways:

(i) Soviet studies have shown that the ratio of maximum snow accumulation depth to the average yearly maximum snow depth is 1.43 for "open field" conditions (Pupkov 1964). In the model, this ratio is equivalent to the maximum snow depth in D experiments to the maximum depth in the control. Over most of Asia the model ratio was typically 1.5–1.7, a value in good agreement with the observations.

(ii) The observed ratio of snow depths in "heavy" snow years to "light" snow years is between 2 and 5 for most of Asia. The ratio of model D to H snow depths averaged over Asia, a number comparable to Rikhter's (1954) ratio, is 2.9 in April and 4.2 in May; again a good agreement.

(iii) The absolute snow depth (water equivalent) differences between D and C runs for April–June averaged over Asia was 13 cm, 16 cm, and 10 cm, respectively. The comparable difference values between the C and H runs was 5 cm, 6 cm, and 2 cm, respectively. Fourteen years of data from 18 stations scattered over central Asia were used to estimate the observed monthly standard deviations in snow depth (water equivalent). There was wide variability between these numbers but they ranged between 0.7–11.4 cm of water equivalent for April and 0.3–9.9 cm for May. Limited observations precluded an estimate of interannual variability for June. Inspection of individual values for specific locations suggest that the D experiments correspond to a 2–3 sigma anomaly while the H experiments are a one sigma event. In short, the perturbation experiments seem realistic.

(iv) During June the snow depth difference between D and C experiments averaged over Asia was 10 cm. The heat required to melt and evaporate this amount of snow is equivalent to that required to create an ocean temperature anomaly of 1°C extending to a depth of 65 m; such anomalies are commonly seen in the oceans. Thus, the amount of thermal potential energy in the anomalous snow pack seems very reasonable.

In summary, the relative size of the perturbations during the D and H experiments relative to the control is comparable to those observed in nature. Since we are comparing differences between perturbation runs and the control, our results should be relevant to the real world.

b. *Results*

1) REGIONAL RESPONSE

The numerical simulations with varied snow depth over Eurasia produced large, significant changes in the atmospheric variables normally associated with the Asian summer monsoon. In general, *a heavier than normal snow pack over Eurasia (D experiments) led to a weaker than normal, or "poor", monsoon.* A lighter than normal snow pack lead to a stronger than normal, or "good" monsoon. The following paragraphs give a brief descriptive account of the evidence that led to these conclusions and, hence, verification of Hypothesis II.

In the discussion, it was useful to compare composited observed anomaly fields with the model simulations. One set of composites came from the 14 year snow depth data at the 18 Asian stations. The 2 years with the deepest spring snow pack (1979 and 1983) and the 2 years with the shallowest spring snow pack (1978 and 1984) were used to develop composites for the D and H experiments, respectively. We would have preferred to use more than 2 years in the composites but the shortness of the dataset and the desire to study its extremes left us little choice. Thus, while many of the comparisons between model and data to be shown are favorable, one must remember the small number of realizations involved.

It was also convenient to develop composites based on the strength of the Southeast Asian monsoon. The first EOF of 45 precipitation stations scattered across India and Southeast Asia had components of like sign and so represents a signal in the precipitation field that is coherent over the entire region. The three years between 1950 and 1980 with the largest/smallest values of the associated principal component were designated good/poor monsoon years. Good monsoon years were 1956, 1961, and 1970 while poor monsoon years were taken to be 1965, 1968 and 1972. These definitions are in reasonable, though not exact, accord with the definitions of Parthasarathy and Mooley (1978), Mooley et al. (1986) and Khandekar and Neralla (1984) for the Indian monsoon.

Surface temperature

The normalized difference (Δ) between the average of the four D/H experiments and the control run mean [e.g. $(D - C)/\sigma$] are shown in Fig. 6 for the land's surface temperature in June. Values of Δ greater/smaller than $+2/-2$ are common over much of Asia for the H/D experiments for the March–August time frame. The largest signals are seen at the surface in the D experiment with the Δ exceeding 2 over much of Asia. These values correspond roughly to a June surface temperature averaged over Asia that is 3.2°C colder during the D experiment compared to C. Note the region of large negative anomaly lies below (south) of a region of little or no anomaly in May and June. The latter regions are still snow covered in both the D and C simulations. By contrast, the large negative temperatures are associated with regions of either rapid snow melt or areas that have recently become snow free (see below). The large negative anomaly retreats northward with the season until it covers only the northern fringe of Siberia in August (not shown). By contrast, the H experiments have positive surface temperature anomalies; a result of the early snow melt associated with less snow depth and subsequent heating of the land by solar radiation. In this group of experiments, June

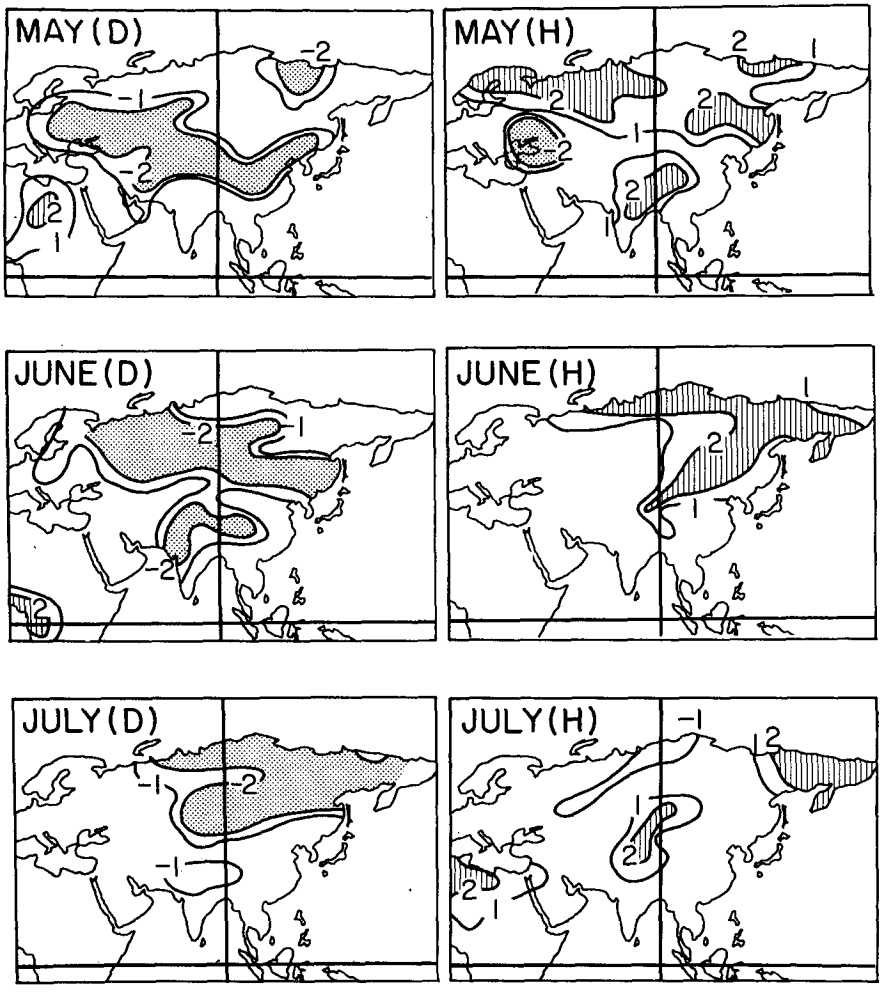

FIG. 6. Normalized difference (Δ) fields between the D and H experiments and the control run for surface temperature for the months of May through July. The regions of stipling or hatching indicate Δ values less than −2.0 or greater than 2.0, respectively. See section 2b for the definition of Δ.

temperatures averaged over Asia for the four experiments were 1.1°C warmer than in C. The spatial distribution of temperature anomalies and their temporal evolution in H is similar to those in D (but of opposite sign) if one allows a one month lag, i.e., the June temperature anomaly field in H resembles that for July in the D experiment. The response in the H experiments closely resembles, but is weaker than, that described by Kutzbach (1981) for the monsoon circulation in the Holocene; a time of reduced snow cover over Asia. By the end of August, the temperatures have largely returned to normal in the H experiments.

Tropospheric temperatures

The entire atmospheric column over much of Eurasia reflects the patterns seen at the surface in the D and H experiments (Fig. 7). The regional Δ values are highly significant, as are those in other regions of the globe [to be discussed in section 5b(2)]. Thus a cold atmospheric column over Eurasia goes with heavy snow cover. The magnitude of the meridional temperature gradient in May/June is of critical importance to the establishment of the monsoon. During typical D and H experiments there is little difference in the 200 mb temperature, approximately 219–220 K in June, over the Arabian Sea/Indian Ocean. However, over the Middle East and Central Asia the net difference between the two experiments is 4–6°C (in June). Thus during H, the meridional gradient is positive with temperature values over the warmest regions of the Asian heartland (229 K) approximately 9°C higher than over the ocean (220 K). During D, the warmest values over Asia are of order 224 K and the meridional gradient is reduced in strength by a factor of two. The same behavior is seen at all levels between the surface and 200 mb. Since it is the strength of these meridional

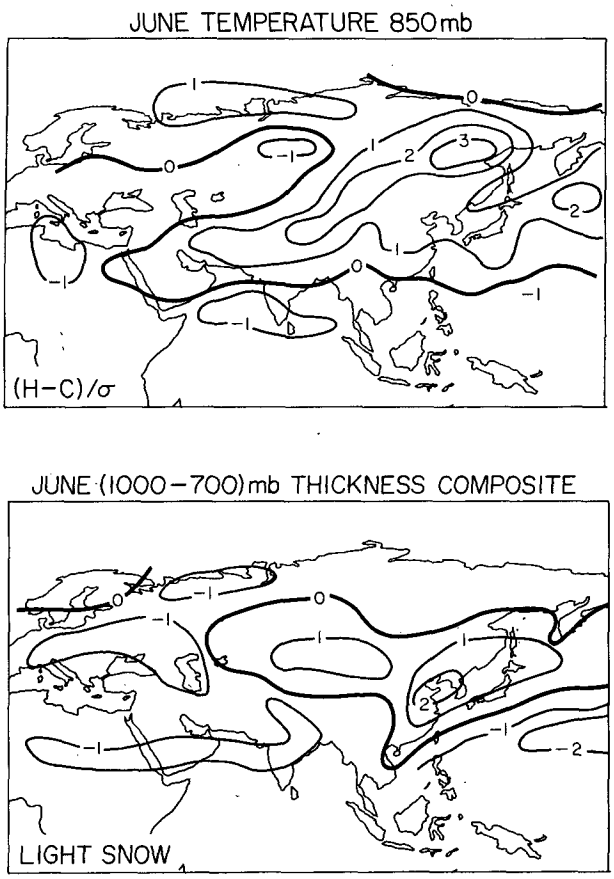

FIG. 7. Top: As in Fig. 6 except for the temperature at 850 mb during the month of June. Bottom: Observed 1000–700 mb thickness anomalies for composited light snow conditions. Units are in standard deviations with $1\sigma \approx 2°C$.

gradients that helps initiate and sustain the monsoon, it is clear the D experiments represent a "poor" monsoon situation and the H experiments the opposite.

The model temperature response at 850 mb is compared against observed temperature, approximated by the (1000–700) mb thickness field over Eurasia (Fig. 7). The light snow composite shows a large region of higher than normal temperature over central and eastern Asia with lower than normal temperatures over Europe, the Middle East and western tropical Pacific. The corresponding results from the H experiments (Fig. 7, top) show a remarkable similarity in spatial distribution. Even the magnitude of the largest anomalies, approximately +2°C, are in accord. Comparison of the thickness composites for heavy snow condition with the D experiments shows lower than normal temperatures over central Asia, again a favorable comparison. However, where the D experiments give an anomaly that is coherent over all of Eurasia, the thickness fields mostly show a dipole response: cold over Asia and warm over Europe. The failure of the model to reproduce this dipole structure may well indicate the zonal extent of our snowfall perturbation is too large. Or it may indicate we have no really large heavy snowfall realizations in the snow dataset. It is therefore with caution that we conclude the model, to first order, compares favorably with observations.

Geopotential height field

The temperature differences between the D and H experiments are reflected in the height fields over Eurasia (as expected). This is illustrated for the 200 mb height field in Fig. 8 (upper panels only). The H ex-

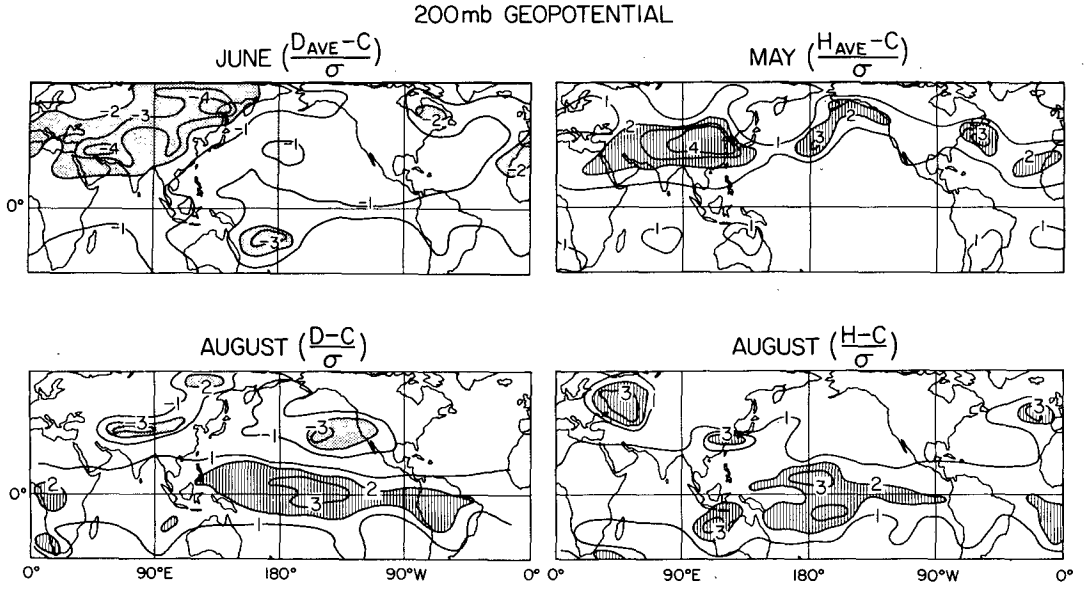

FIG. 8. Upper panels: As in Fig. 6 but for 200 mb geopotential height field in the months noted. Lower panel: 200 mb height anomaly field (August) for a selected D and H run.

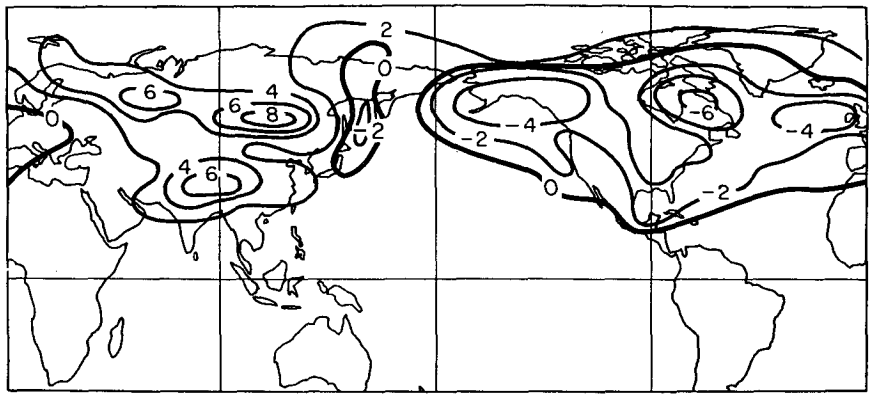

FIG. 9. Average of the June sea level pressure field for the four D experiments minus control (mb).

periments show higher heights than C in the April–July time frame due chiefly to the increase in latent heat release associated with enhanced precipitation and decreased atmospheric albedo. The colder atmosphere (lower heights) is presumably due to less heating but other factors enter also as we shall see in section 6a. The sea level pressure (SLP) behaves as expected: higher than normal pressure over much of Asia during a poor monsoon (D), (Fig. 9), and lower than normal pressure during the H experiment (not shown). Again, the nonregional response will be discussed below as will the comparison with observations.

Wind fields

The Δ values for the zonal surface winds for the D experiment show a decrease over the Arabian Sea and Indian Ocean for the May–August period. These anomalies are of order 1–2 m s^{-1} or roughly 10%–30% of the mean. The decrease in the eastward directed wind component over the landmass of southern Asia is as large or larger. These results suggest a reduction in the surface convergence and are expected during a poor monsoon. There is also a decrease in zonal wind over the Pacific but discussion of that effect is deferred to section 5b.

Surface wind observations over the northern Indian Ocean from ships weakly support the model results. Poor monsoon defined by the Southeast Asia precipitation index years do have (on average) a decrease of about 0.5 m s^{-1} in the zonal wind component. However, this value is quite variable within the main monsoon season. In some poor monsoon years (e.g., 1982) even the sign of anomaly is reversed. The changes in winds over the land mass seem to conform, at least qualitatively, to observations noted by Blanford (1884). Composites based on the snow depth index agree more closely to the model prediction with reduction of 1–2 m s^{-1} for heavy snow cases and increase of 1 m s^{-1} for the light snow cases.

The modeled behavior of the zonal component of the wind at 200 mb in the tropics from May through July showed just the behavior expected from observations (Tanaka 1980; Hastenrath 1985). During the D experiments (poor monsoon), the development of the tropical easterly jet (TEJ) is weak and of limited spatial extent. This is shown as a region of positive anomaly in the June zonal wind at 200 mb (Fig. 10, upper). During the H (good monsoon) experiments

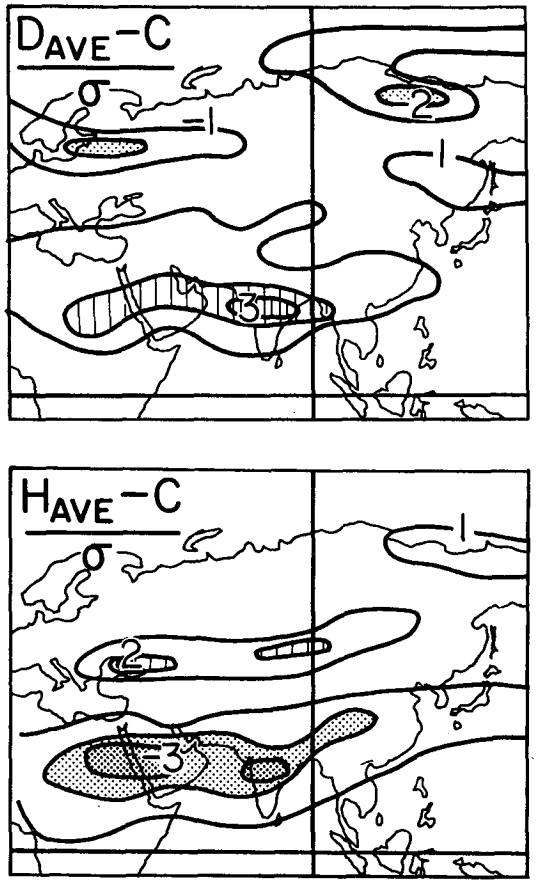

FIG. 10. As in Fig. 6 except for the zonal component of the wind at 200 mb in June.

the jet was stronger and of greater longitudinal extent (Fig. 10, lower) as expected from observational studies. Typical differences in the zonal wind at 200 mb between the D and H experiments in June are approximately 10 m s^{-1}; a number in good accord with the observations of Tanaka (1980) for the range between good and poor monsoons and Kutzbach (1981) for the TEJ associated with the Holocene monsoon system. Note also the decrease/increase in the midlatitude jet over Asia during D/H experiments.

Precipitation

The actual precipitation differences between the average of the four D runs and C for June and July and between the average of the four H runs and C for May and June are shown in Fig. 11. The one-month offset accounts for the phase difference between the maxima in the experimental responses. The PPP tests applied to the Asian precipitation fields between the D and C experiments show them to differ from each other with confidence > 98% between May and August. The H and C precipitation fields were also different from each other with confidence > 98% between March and July. Further, the areal sense of the anomalies is as hypothesized: less precipitation over Southeast Asia during all D experiments and more during all H runs. Also, the maximum anomaly occurs where the observed rainfall is a maximum, i.e. in the heart of the Asian monsoon.

Comparison of the model precipitation with observations again produced a reasonable agreement. The snow depth composites gave the results in Fig. 12. The observed precipitation anomaly has the correct sense as predicted by the model. However, the magnitude is generally a factor of 2–3 less than the model values but again, the composite consists of only two realizations. A separate investigation showed the heavy/light snow composite years were also poor/good monsoon rainfall years according to the all-Southeast Asia precip index. Both results support the model result that heavy Asian snow cover precedes a poor monsoon.

One apparent peculiarity in the precipitation field is the occurrence of *more* than normal rain in western India and Pakistan and Afghanistan during June in D experiments. During the H experiments, this region tended to have less precipitation than found during C but the signal was small and below the 5 cm contour level. The numerical experiments thus suggest a dipole signal in the experimental precipitation response although the western (desert) end of the dipole is small (only a few model grid points), weak, and represents relatively small amounts of precipitation compared to the main (eastern) lobe of the dipole. The EOF analysis performed on the station precipitation data for South-

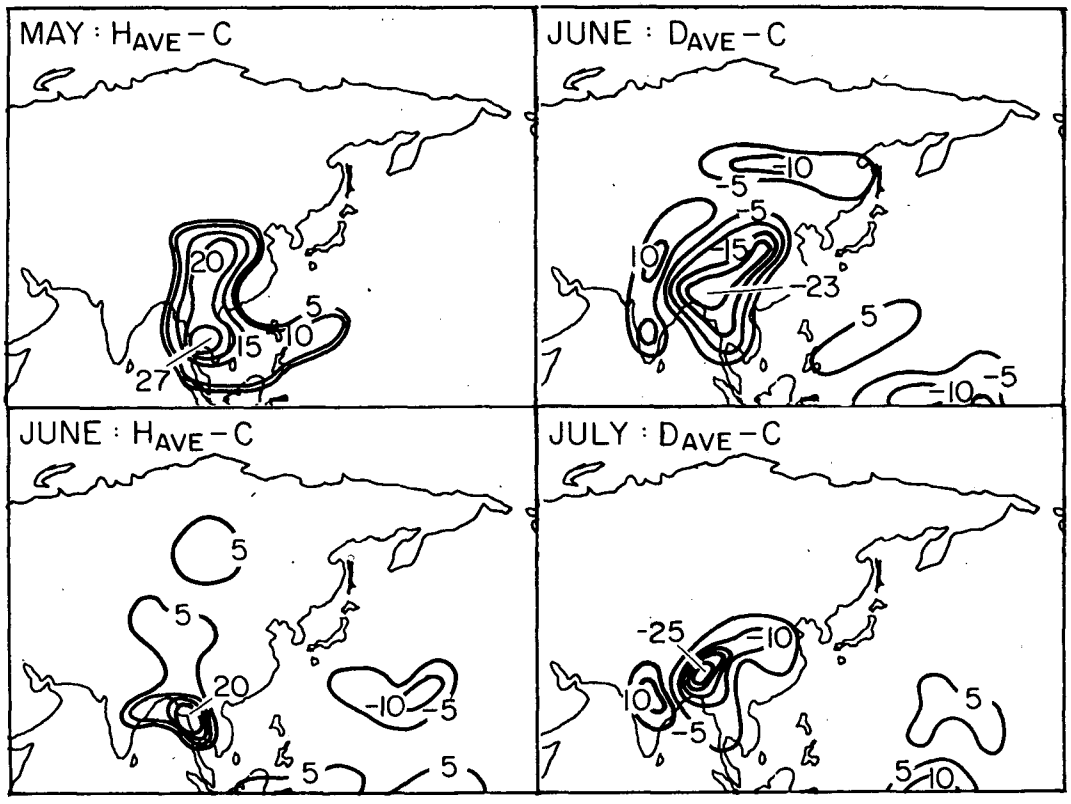

FIG. 11. Difference in precipitation between the average of the four D/H runs and control for the months shown. Units are cm.

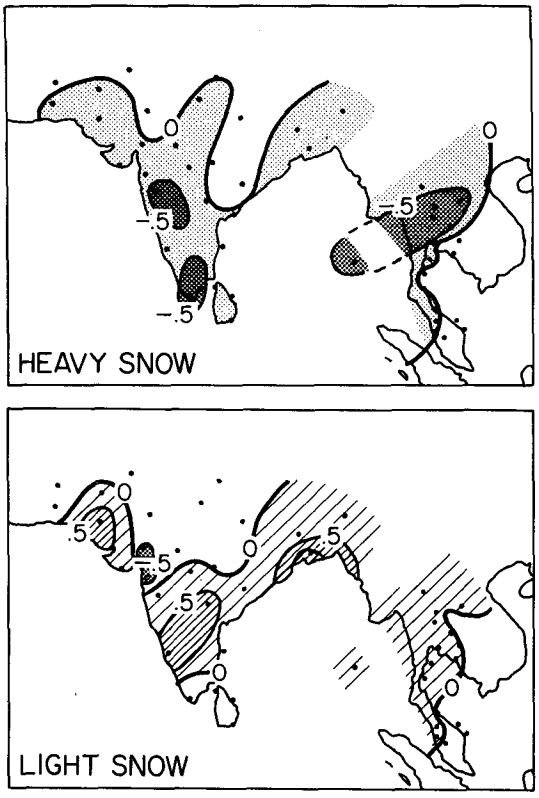

FIG. 12. Observed monthly precipitation anomalies for heavy and light snow year composites. Units are in standard deviations.

east Asia shows this dipole pattern to be the second most energetic mode of rainfall variation; nearly as strong as the leading mode which was a monopole. The more spatially limited analysis of Weare (1979) also hints at the existence of the dipole. It appears the model has produced a real feature of the Asian precipitation field, although not necessarily one that is generally associated with "good/poor" Indian monsoons. The main model response was, however, exactly what one would expect for "good/poor" Southeast Asian monsoons. These results emphasize the fact that our results pertain to the Asian monsoon in its entirety and not to the subelements, e.g. "Indian" monsoon. The model resolution is not adequate to discuss these small scale systems.

Soil hydrology

A crucial item in the experiment will turn out to be the differential behavior of the soil moisture during the D and H runs. The surface soil moisture content (Fig. 13) illustrates well the time lag between comparable states of the D and H experiments. In the light snowfall case, most of the snow is gone over central Asia by the end of May and the soil moisture is being evaporated. Thus the soil moisture content is less than normal over most of Eurasia (March–July); except in areas where snow is still melting and/or on the ground. By June the large standardized anomalies are gone in central Asia. Inspection of the actual values shows this result

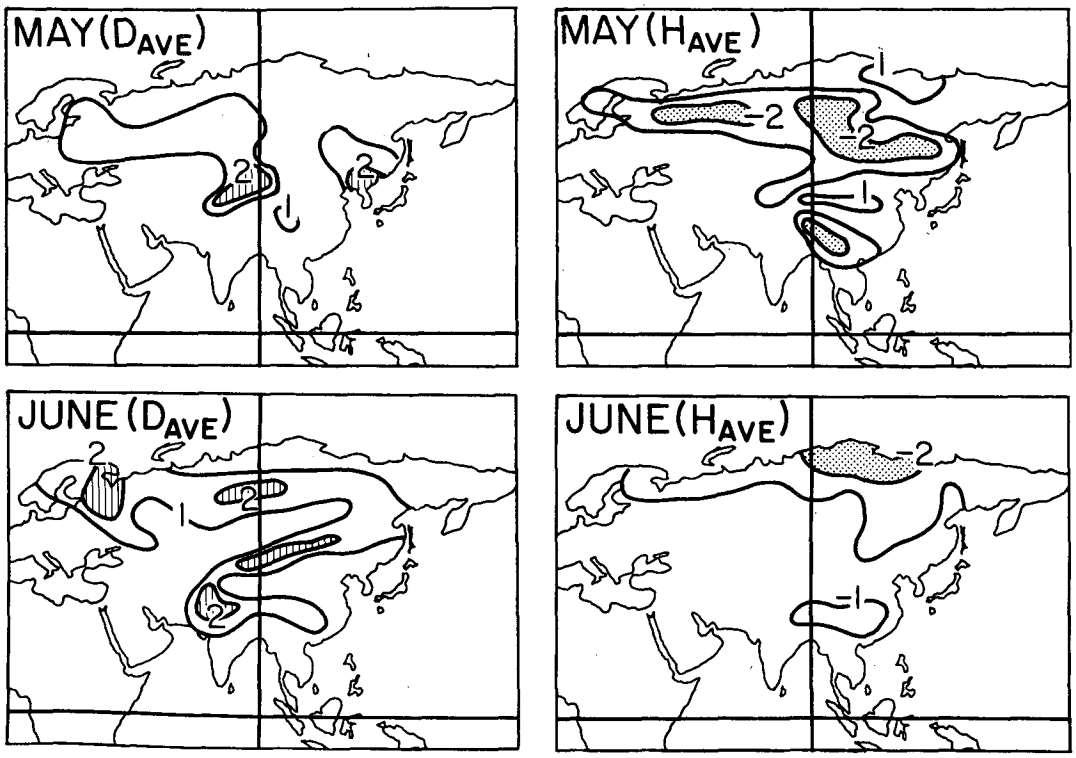

FIG. 13. As in Fig. 6 except for the soil moisture in the surface layer of the soil model.

is due to a nearly complete utilization of the surface moisture in these dry regions of Asia. In the D experiment, by contrast, the standardized anomalies are largely positive (April–August) reflecting (i) the increased moisture available through prolonged, excess snow melt and (ii) the protective effect of the snow cover that lasted later into the seasonal cycle than usual.

The anomalous soil temperature reflects almost exactly the surface temperature (ref. Fig. 6) in both spatial distribution and magnitude. In some areas, the deep soil temperature, which is closely tied to a fixed climatological value, was even 1°–2°C warmer than that in the surface layer during the D experiment. The difference in the June temperature averaged over Asia of both the surface and deep soil between the D and H experiments was approximately 4.3°C.

In summary, the D experiment had significantly more ground water over much of Eurasia later into the seasonal cycle than during either the control or H experiment. This water was considerably colder than during C. In the H experiment, the early removal of snow led to earlier availability of ground moisture to the evaporation process. This moisture was also warmer than expected relative to the seasonal cycle.

2) REMOTE RESPONSE

The original thrust of our studies was aimed at regional climate dynamics but the results of the D/H runs showed large-scale responses in regions of the globe far from Southeast Asia. This section describes several of the strongest of the remote responses.

Asian–North American teleconnection

The occurrence of higher than normal SLP over Asia during the D experiments is accompanied by a large area of lower than normal SLP over North America and its surrounding oceans (ref. Fig. 9) The PPP tests confirm the high significance of the response over North America. We conclude the feature represents a real difference between the D and C runs. More or less the opposite (significant) response was observed in the H experiments. These responses are highly reproducible from experiment-to-experiment.

The teleconnection is most strongly manifest in the D experiments in June with the largest individual SLP anomalies over North America lying in the range −4 to −6 mb. In contrast the anomalies over Asia are +6 to +8 mb. The initiation of the positive lobe of the dipole over Asia coincides with the start of the snow melt season but lingers through September well after all snow has melted. The negative lobe first appears in May over the Aleutians and has vanished, even reversed sign, by August. The pattern clearly represents a major readjustment of the atmospheric mass field in the middle to high latitudes of the Northern Hemisphere.

Is the teleconnection pattern produced by the model observable in nature? We took three approaches to answering this question:

(i) The SLP composite for the heavy snowfall years gave only modest agreement with the model results. The SLPs over Asia were generally positive but smaller (1–3 mb) than the model values. The structure over North America was not well reproduced. It is important to remember these composites are based on but two years and one of these (1983) was extreme in many ways.

(ii) The poor Southeast Asia monsoon composite (Fig. 14) gives somewhat better comparison (cf. Fig. 9). Positive anomalies are seen over much of Asia but they are not uniform nor as large as the model simulations. The low off Kamchatka is reproduced as is the structure over North America. Again, however, the composite anomalies are weaker than the model response, the low over the Atlantic displaced eastward and the ridge over the eastern part of the North American continent stronger than in the model.

(iii) We next formed composites for the five years with highest observed SLP averaged over Asia (1957,

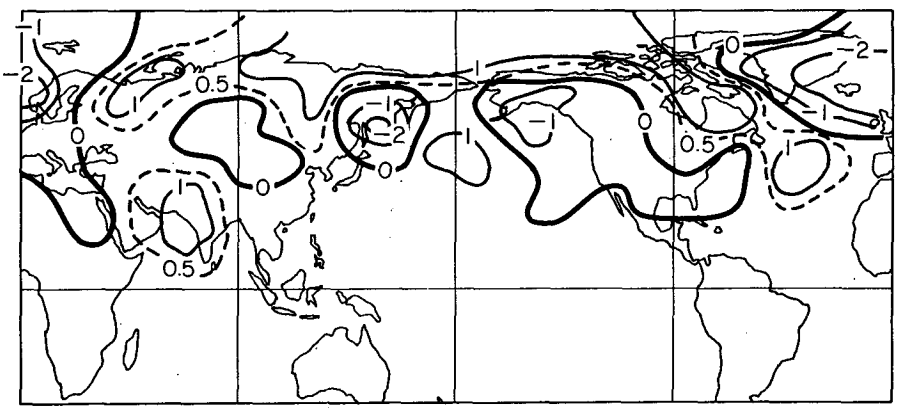

FIG. 14. Composite SLP field anomaly from observations for three relatively poor monsoon years. Units are in millibars. These results can be compared directly with the model response given in Fig. 9.

1958, 1959, 1972, and 1982); four of five which were ENSO years. The results were quite similar to those shown on Fig. 14, if not better. We also formed composites for the opposite atmospheric state over Eurasia, i.e., the three "best" monsoons and five years with lowest surface pressures. The results (not shown) follow fairly well those shown in Fig. 14; low pressure over Asia and high pressure over the eastern Pacific and western Atlantic. This was essentially the response observed in the H experiments.

In summary, some features of the large scale model SLP signal are observable in SLP data composited in various ways. However, the signal in the real world is neither as strong or as consistent as in the model. The composite results sensitivity to different selection criteria is stronger than we would wish. It is concluded that the large-scale SLP signal produced in the model is likely to be real but certainly not as strong as suggested nor as reproducible in nature on an event-by-event basis.

The Asian–North American teleconnection at 200 mb also was highly significant (>95%) but suggests a different midlatitude structure than at the surface (ref. Fig. 8, upper panels). The anomalies, though weak, now have the same sign over both major Northern Hemisphere continents. Thus the sign of the SLP and 200 mb height anomalies over Asia are opposite suggesting the importance of barcolinic processes in that region. Over North America, however, the anomalies suggest a barotropic response. The development of these patterns in all D and all H experiments is highly reproducible until August when the midlatitude features fade to insignificance. Further, the midlatitude anomalies between the D and H experiments are largely mirror images of each other suggesting a rather symmetric midlatitude response to the anomalous Eurasian forcing (see section 6b).

Large-scale tropical response: Upper levels

The model's large-scale response in the tropics suggests the existence of two preferred, unstable states in its internal climate. These states are best defined and most obvious in the 200 mb height field of the D experiments (Fig. 8, left upper). Ignoring the midlatitude teleconnection discussed above, the states are seen to occur in the deep tropics and are represented by anomalous high or low geopotential heights at 200 mb. This signal is more or less symmetric about the equator and coherent around the entire tropical strip.

The direct linkage to Asia is obvious in the study of individual D/H runs during the time of maximum monsoon perturbation. However, either state could be found also sometime during the summer months in either the D or H experiments and this is illustrated in the lower panels of Fig. 8. Indeed, both states occurred in both sets of numerical experiments after the snow-induced forcing subsided, e.g. a "high" state might occur in either a D or H experiment from August onwards. In all cases, the responses were large relative to the control standard deviation but significant only in June when the PPP methodology was used. This apparent significance dichotomy is resolved in section 6b. Note the coherent model signal around the entire tropical strip at 200 mb is typical of those found in nature during the winter months of ENSO events (Horel and Wallace 1981; Barnett 1985b).

The anomalous states described above had life times of several months, which suggests they are not associated with 30–50 day wave phenomenon. These waves do exist in the T21 model but have relatively short periods; 24 days being typical (von Storch et al. 1988). Interestingly, the only significant anomalies found in the tropical 200 mb height field were associated with these states. When a given state was obviously related to the monsoon perturbation, then it took the sign of the 200 mb height over Asia—a polarity expected from the precipitation anomaly, i.e. heavy rainfall (large heating) going with positive height anomalies and vice versa. When the forcing from Asia was nil, the two states occurred with equal frequency and equal polarity in *both* D and H experiments. In these cases, the anomalies attained maximum amplitude in either the western or central equatorial Pacific.

Large-scale tropical response: Surface

A number of surface fields demonstrated a marginally significant response between the D and H experiments over the tropical strip of the Pacific Ocean. The surface heat fluxes, both sensible and latent, decreased during the D experiments relative to the control. This resulted from a weakly significant (~90%) decrease in the surface wind velocity in D relative to C. An example of this result is shown in Fig. 15, where the u-component averaged between 106°E and 152°W, is shown as a function of latitude and time. The general weakening of the wind in the Southern Hemisphere and along the equator is typical of the D-experiments. This response is similar in nature to that expected prior to the warm phase of ENSO events (e.g. Barnett 1977). During the H experiments, the signs of the anomalous changes reversed and the easterlies strengthened; a condition typical during the "cold phase" of an ENSO event.

The responses in the surface fields discussed above were generally only significant in May and/or June. Similar but weaker signed anomalies existed for 1–2 months on either side of the significant months. Thus, the model responses do agree qualitatively with observations during ENSO/non-ENSO events. But one must be cautious in accepting the results due to their low magnitude. We shall return to the potential role that these surface responses might play in affecting the ocean in section 7.

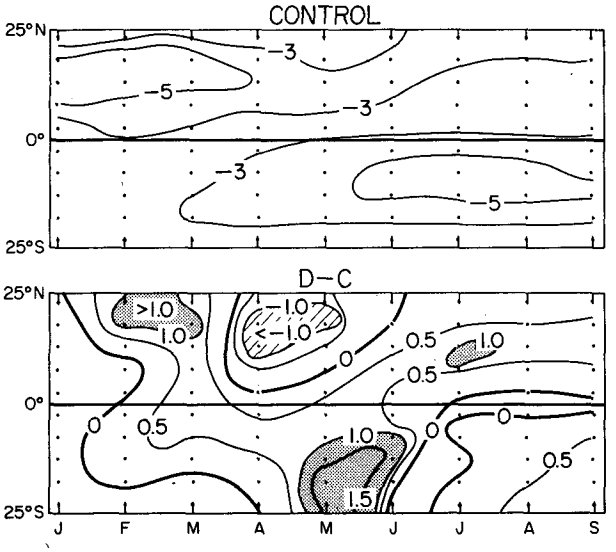

FIG. 15. Zonal wind component (m s^{-1}) averaged along latitude lines from 106°E to 152°W for the months of January through September. The upper panel shows the average value for the 10-year control run. The lower panel shows the result of subtracting the control values from those obtained during a typical D experiment.

6. Physical mechanisms

There has been considerable speculation regarding the mechanisms by which large-scale snow fields might affect the atmosphere. In the case of the Asian monsoon, reference is often made to the role of the Tibetan Plateau acting as an elevated heat source forcing the reversal of the circulation by season (e.g. Flohn 1957; Webster et al. 1977; He et al. 1987). The design of our experiment and resolution of the model is such that the forcing is not confined to the Tibetan area alone, but to a larger part of the Eurasian continent. Further, our simulation actually deals with the entire Asian monsoon of which the oft-studied Indian monsoon is but one element. With these items in mind, we discuss first the physics responsible for the regional response described in section 5b and then the causes of the remote responses.

a. Regional physics

The physical processes that conspire in the model to control the land–ocean temperature contrast, and hence the summer monsoons, seem to work in stages depending on the state of the snow pack and phase of the seasonal cycle. Let us concentrate initially on the physics operative in the D experiments:

(i) When excess snow is present the dominant terms in the surface heat balance are shortwave (solar) radiation (S) and latent heat flux (Q_L). The increased albedo of the snow reduces the S received by the landmass. But the sublimation of the snow is generally less than evaporation from the soil, plus the ground and air are colder and surface wind reduced so Q_L is reduced. These two terms largely cancel each other, leaving generally a small positive (land warming) residual. The smaller sensible heat flux (Q_S) and longwave radiation (IR) anomalies are positive due essentially to the colder surface temperature and also represent anomalous warming of the landmass. These results are illustrated in Fig. 16 which also shows the spatial complexity of the flux fields.

The total surface heat balance ($S + \mathrm{IR} + Q_L + Q_S$) is positive for regions of active snow melt, typically 20–40 W m^{-2} (Fig. 17).[2] Instead of warming the land surface, this small positive flux anomaly is used as heat of fusion to melt the snow pack so that the land itself remains cold longer into the seasonal cycle during the D experiments and hence can be thought of as a heat sink. Since less heat is transmitted to the atmosphere the air temperatures also remain cold. In practice, the flux anomaly is used first to melt any snow that might still be on the ground if the soil temperature is greater than 0°C. If no snow remains, the soil is warmed by the appropriate amount.

(ii) As the snow disappears several additional factors work to keep the landmass cold and prevent or diminish establishment of the meridional temperature gradients needed to initiate a vigorous monsoon. The excess cold melt water keeps the soil saturated and chilled longer into the seasonal cycle than normal. The evaporation of this moisture further keeps the near-surface temperature low. In the model, the soil processes are represented in three layers which communicate via diffusion processes. Suffice it to say, the time scale of this communication is such that evaporation cannot quickly remove the moisture anomaly, so the soil will remain cold and moist well into the summer season. It is this feature of the physics that provides a "memory" in the system. Hence, the maximum of land surface temperature occurs about one month later in the D experiments than the H runs. The timing is critical, particularly at high latitudes, for after the summer solstice (23 June) the solar radiation available to the evaporative process and to warm the land/atmosphere begins to diminish. The above findings are similar to those of Yeh et al. (1983) from a simplified modeling study.

Since much of the evaporation occurs over moderately arid regions it does not immediately feed back heat to the atmosphere via precipitation as might normally be thought (e.g., Meehl and Washington 1987). Thus, the atmospheric column above the surface boundary layer does not warm by latent heat release. More importantly the increased atmospheric moisture results in a deficit of net energy ($S + \mathrm{IR}$) being absorbed by the entire atmospheric column. In this case, the

[2] The above picture is complicated in the case where snow has all melted in the control run but still persists in the D run. In this case, the albedo changes allow S to dominate the surface budget.

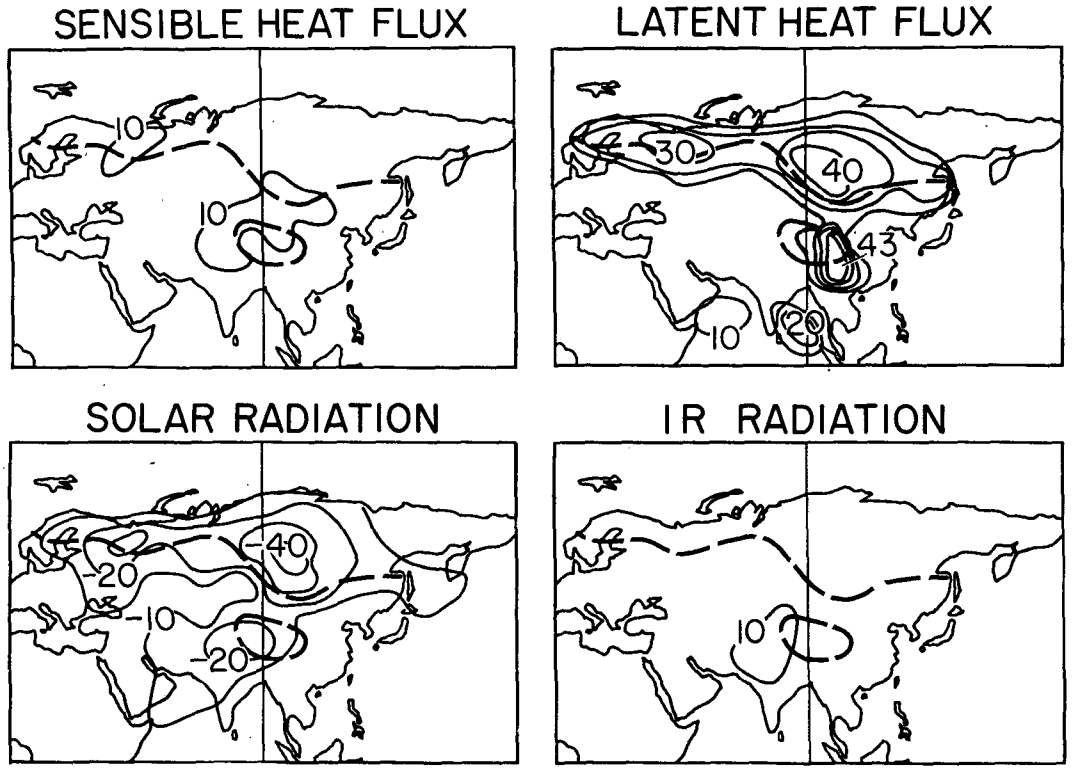

FIG. 16. Components of the surface heat budget for the averaged D experiments minus control for June (W m^{-2}). The dashed line is the approximate position of the snow line in the model. Positive/negative values represent fluxes into/out of the earth/ocean surface.

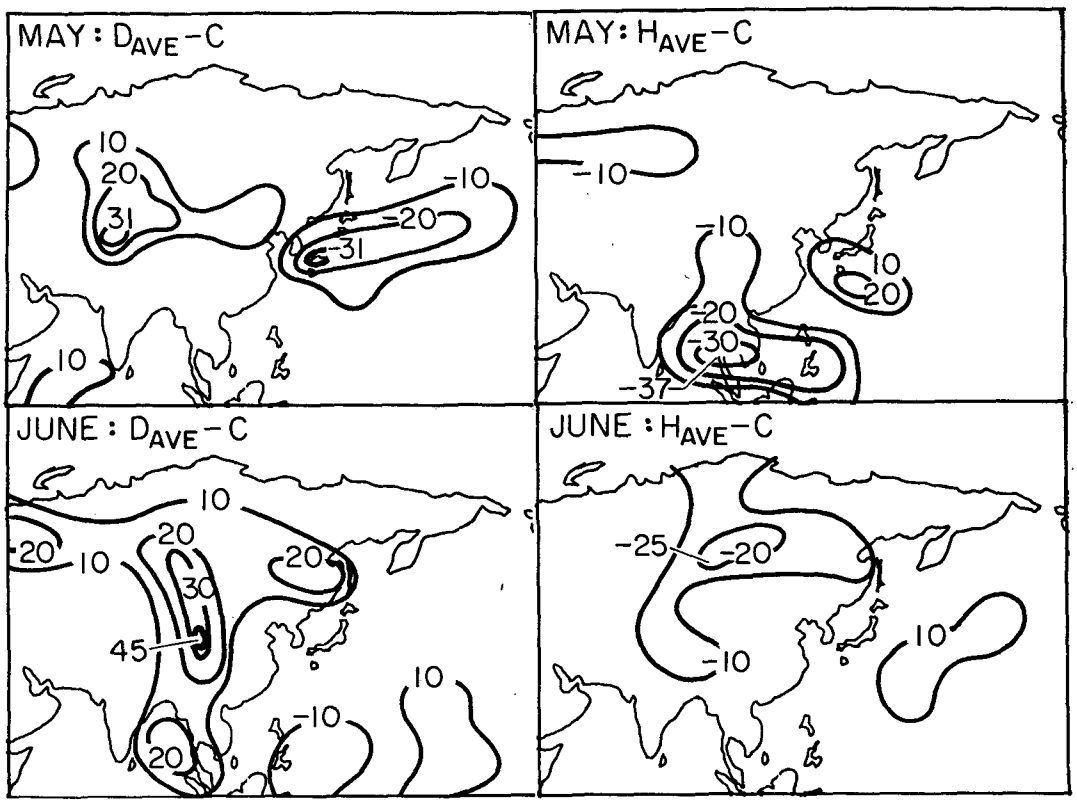

FIG. 17. Difference in net surface heat flux over Asia and surrounding oceans between D/H experiments and the control (W m^{-2}).

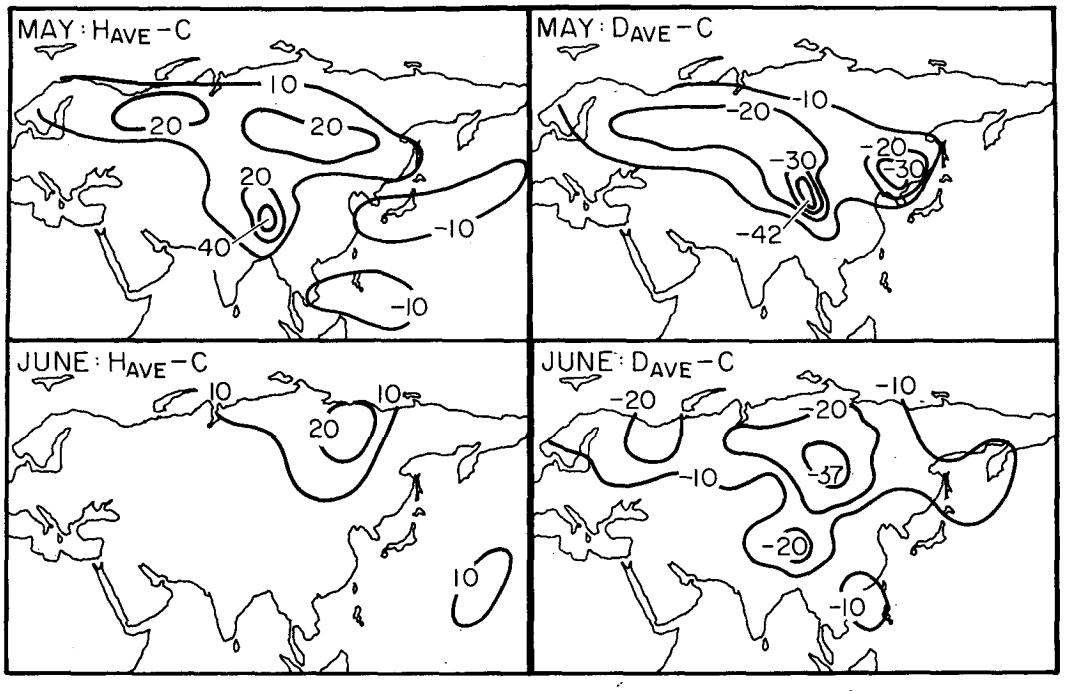

FIG. 18. Difference in net heat flux (solar + IR) at the top of the atmosphere between D/H experiments and the control (W m^{-2}).

increased effective albedo (clouds) reduces the solar radiation gain more than the cold atmospheric temperature reduces the IR loss. The net loss (S + IR), averaged over all of Eurasia, is largest in May and June, relative to the control attaining values of −25 to −30 W m^{-2} during the D experiments and with slightly smaller, positive values occurring during the H experiments (Fig. 18). This anomalous net energy outflow from the atmospheric column is of order 30% of typical net values in the control run and so acts as a powerful mechanism for keeping the atmospheric column cold. Interestingly, satellite estimates of the anomalies in net total heat flux from the top of the atmosphere suggest values of order 10–30 W m^{-2} during poor monsoon conditions (Fig. 19, courtesy of J. Winston, personal communication); a result in unexpectedly good agreement with the model estimates given above, provided one allows for the one month temporal phase shift associated with the somewhat tardy retreat of the model snow line, i.e. compare April observations (Fig. 19) with model data for May (Fig. 18, upper right).

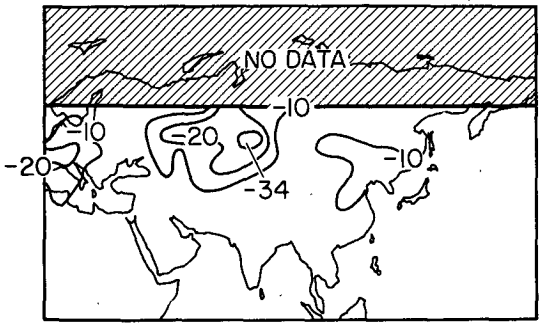

FIG. 19. Net flux anomaly (W m^{-2}) observed by satellite during April of the poor monsoon year of 1979. Data courtesy of J. Winston.

Another process important to the monsoon cycle is the heat and moisture anomalies evident over the surrounding oceans (Fig. 17). In May, during D experiments, larger than normal ocean-to-atmosphere fluxes are found off the east coast of Asia; a consequence of colder than normal air being advected over the warm ocean. In June, this situation changes as the mean air flow reverses sending marine air into the continent. More interesting are the anomalous fluxes over the northern extremes of the Indian Ocean. These anomalies are due almost entirely to Q_L. According to typical bulk formulations the reductions in wind speed over the oceans [section 5b(1)] will reduce Q_L during D experiments. In a sense, this is a positive feedback process since decreased Q_L over the oceans leads to less moisture available for monsoon precipitation and less heat release in the lower atmosphere. This, in turn, helps to maintain a decreased land–ocean temperature contrast in the upper atmosphere and gives rise to a weaker convection cell and eventually a weaker surface flow over the oceans, which completes the feedback cycle. It is interesting that by keeping the atmosphere over the land mass cold, the snow perturbation has effectively put a cap on the large-scale Asian heat and mass sources at upper levels.

A final major process vital to the regional response

is obviously the anomalous heat flux associated with the variations in precipitation (cf. Fig. 11). Local flux values of 100–300 W m^{-2} may be inferred from the size of the precipitation anomalies. However, the smaller fluxes from the continent discussed above will, when averaged over all of Asia, tend to dominate over this more intense, small scale precipitation related signal.

During the reduced snowfall (H) experiments, the sequence of processes works in much the same fashion noted above except the signs of the anomalous fluxes, etc. are reversed. Both the spatial distribution of anomalies and their magnitudes are much the same (see below).

The major difference between the D and H experiments is one of timing. The scenario described above is largely over and conditions over Eurasia have returned to normal by the end of August in the D runs. In the H runs, conditions over Asia have become indistinguishable from the control run by the end of July. Similarly the anomalous events begin about one month earlier during the H runs than for D runs; typically March compared to April.

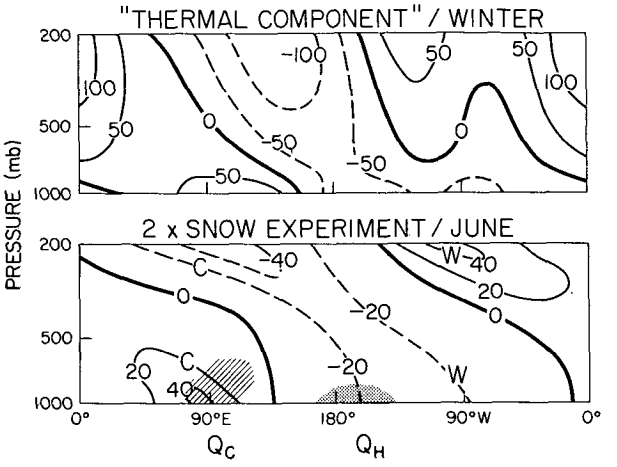

FIG. 20. Lower: The vertical and zonal distribution of geopotential height anomalies (after removal of a zonal mean) simulated for June in the D experiments. The C/W symbols indicate colder/warmer temperatures than in the zonal mean control. The maximum heating anomaly is located at "Q_H" and denoted by stiple while the maximum cooling anomaly is at "Q_C" and denoted by hatching. In this example, $Q_C \approx 3Q_H$. The contours are meters. Upper: Winter geopotential anomalies (after removal of a zonal mean) from a GCM experiment with "thermal" forcing only. (After Held 1983).

b. Physics of remote responses

Asian–North American response

The (D–C) model's geopotential and temperature fields for June have been integrated between 25° and 55°N. The average geopotential field is shown in Fig. 20 (lower) after removal of a zonal mean.[3] The comparable temperature distributions are indicated schematically [e.g., Cold (c) or Warm (w) on the illustration. The cold surface high over Asia is complimented by a warm surface low over the western hemisphere. Note the sign of the surface pressure anomalies is out of phase with the sign of the temperature anomalies. The height anomalies switch sign by 200 mb but the temperature signatures at 200 mb are largely the same as at the surface. These results suggest that the Asian–North American teleconnection can be explained as the quasi-stationary response of the atmosphere to large-scale thermal forcing. In this case, the response takes the form of an ultralong, baroclinic wave ($k = 1$).

Using the net heat flux at the top of the atmosphere and the net surface heat surface flux, we next computed the effective heating/cooling of the atmospheric columns. The largest heating was found near the dateline and is indicated by Q_H on Fig. 20 (lower). However, appreciable heating was also evident immediately off the east coast of Asia, a result expected when colder than normal air moves over the Kuroshio and Kuroshio Extension. The maximum heat sink (Q_C) was over the heart of the Asian continent as expected.

Results similar to those shown above have been obtained by other investigators in numerical and theoretical studies. For instance, Held (1983) obtained nearly identical results (Fig. 20, upper) for GCM simulations of the winter geopotential field using only the thermal forcing associated with land/sea contrasts (no orographic forcing); a result in concert with the seminal work of Smagorinsky (1953). Roads (1981) found results similar to ours for an idealized snow albedo model that included land and sea contrasts. Thus the result found in our experiments is one more example of the atmospheric responses to large scale thermal forcing.

Based on the results shown in Fig. 20 (lower) and the prior studies noted above, the observed model response can be explained as a balance between advection and local heating (cf. Roads 1980; Held 1983). Since the low pressure anomaly downstream from Q is warm, we infer that the scale height of the heating ($Q/(dQ/dZ)$) is small and so the zonal component of the advection dominates the meridional component (cf. Held 1983). Vertical motions are obviously important in the advective balance also. This fits nicely the physical picture of cold air being advected from the continent over the ocean and being subsequently warmed most strongly in the lower layers of the atmosphere nearest the heat source. Put another way, the cooling of the Asian landmass has simply intensified the ocean–continent temperature contrast and hence the good agreement between the panels of Fig. 20.

[3] Removal of the large zonal mean in the upper levels of the geopotential field makes the dipole signal more obvious. It also suggests that wave–mean flow interaction may be important in fully understanding the response pattern.

In conclusion, we note that the response shown in June is but a snapshot of a teleconnection pattern that undergoes substantial modification between its inception (May) and demise (July) as noted in Section 5b(2). This is expected since the initial forcing from the snow field is itself undergoing major changes in position and strength as the snow line recedes northward (cf. Fig. 17 and 18).

Large-scale tropical response: Upper levels

The large-scale response at 200 mb in the tropics appears to be a natural mode of variation in the T21 model and the real world also (cf. Horel and Wallace 1981; Barnett 1985b). In our simulations, it appears to be stimulated by anomalous thermal forcing of two types:

(i) One forcing mechanism is snow-related precipitation anomalies over Southeast Asia. The associated increased/decreased latent heat release drives the sign of the tropical response, i.e., increased latent heat release warms the troposphere by about 1 K and leads to positive height anomalies at 200 mb and vice versa for the D set of experiments. Thus the response can be viewed as a direct thermal forcing resulting ultimately from the anomalous Eurasian snow cover and the ability of the land surface to perpetuate this anomaly.

(ii) The large-scale response still occurs after all signs of anomalous forcing over Eurasia have disappeared. In fact, a detailed study of the 10-year control run showed the large scale 200 mb tropical response to occur frequently during that integration. In these cases, however, the signal is more or less symmetrical about the equator with little midlatitude component (cf. Fig. 8, lower). It was for this reason that the significance of this response was modest (except in June) using the PPP methodology for the same signal tended to occur in the D, H, and C runs.

The 10-year control run's 200 mb height field and associated potential forcing mechanisms were subjected to a canonical correlation analysis (CCA, ref. Barnett and Preisendorfer 1987). The CCA finds the best linear relationship between any two fields of data. In this case, the 200 mb response was most strongly related to large-scale ($\sim$1000 km) variations in the precipitation field. Although the 200 mb response was more or less coherent in the entire equatorial strip, the CCA analysis showed the forcing was strongly localized between 90°E and the dateline and between the equator and 15°–20°N. Thus, the 200 mb fluctuations in the control run are the result of forcing from large-scale, *stochastic* variations in the Indo-Pacific precipitation field unrelated to any snow, SST, or other imposed variation.

The magnitude of the latent heat release associated with the precipitation variations was adequate to give the observed $\pm$1 K temperature changes. Interestingly, the CCA showed that the precipitation variations were often accompanied by large-scale air–sea heat exchange variations, dominated by Q_L, in the immediate locale of the precipitation anomaly. The sense of the air–sea heat exchange is in concert with the sense of the latent heat anomaly, i.e., increased air–sea flux supports increased precipitation. However, the air–sea exchanges are of order 30 W m^{-2} and can only support about 25% of the latent heat release; a result in agreement with the suggestions of Cornejo-Garrido and Stone (1977) and a value surprisingly close to that estimated by Shukla and Wallace (1983) from model simulations. The remainder of the required energy must come from the moisture flux convergence; a result in agreement with both sets of authors. Finally, it appears there may be a modest lag between anomalous forcing and atmospheric response although we cannot confirm this with the monthly averaged data used in this study.

Large-scale tropical response: Surface

The surface response can generally be attributed to modulation of the large divergence region associated with the Asian monsoon. This is illustrated in Fig. 21, which shows the upper level divergence field for a typical D/H experiment. Note that in May, particularly, the vergence is substantially weakened and displaced eastward in the D experiment as opposed to the H experiment. More modest, yet similar, differences are apparent in June. A simple continuity argument can be invoked to explain the decrease in the near-surface flow field associated with the decrease in upper-level divergence. Hence, during the D experiment, the Walker cell over the Pacific is reduced in intensity (plus displaced eastward); a condition again reminiscent of the warm phase of an ENSO event. Given the weakness of the remote surface response we will defer further analysis of their causes.

7. Relation to ENSO events

a. Overview

A fundamental question raised by many of the results presented above is the role that regional climate variations over Southeast Asia might play in ENSO events. We have established the close link between snow cover/monsoon variation and that was a key link in the suggestions by Barnett (1985a) regarding the evolution of near-global SLP anomalies. Further, the empirical studies mentioned in the Introduction offer strong evidence for a near-simultaneous relation between variations in Indian monsoon rainfall and ENSO.

However, the work reported in the prior sections failed to establish conclusive evidence for a monsoon–ENSO relationship for the following reasons:

(i) The climate variations associated with snow/monsoon perturbation have a time scale of 3–4 months; far shorter than the ENSO cycle. In the observational study of Barnett (1985a) the large-scale SLP

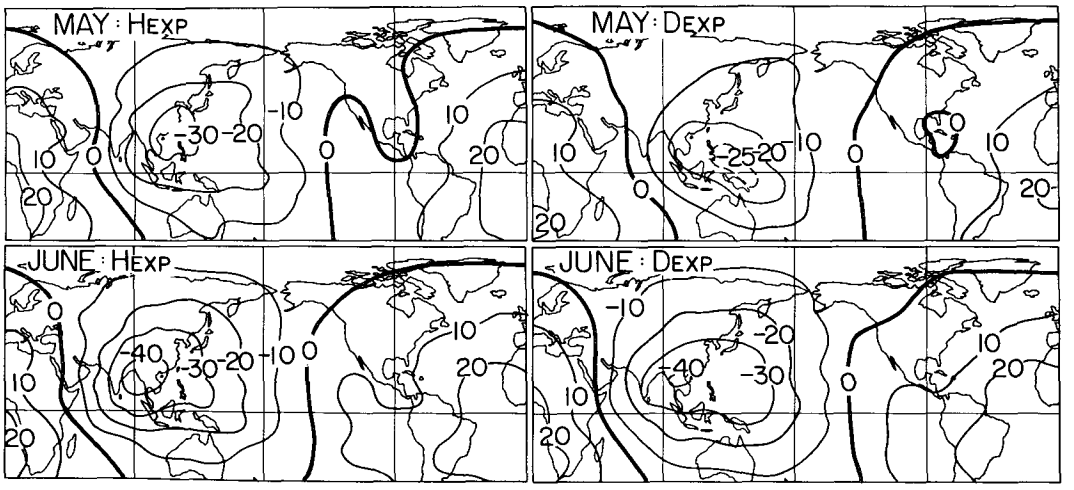

FIG. 21. Divergence at 200 mb for May and June from a typical pair of D and H experiments (relative units).

anomalies developed over Asia in the spring just as simulated here. However, they then expand and intensify during the early summer eventually covering much of the eastern hemisphere. Our simulations did not reproduce this latter effect.

(ii) The large-scale tropical responses away from the monsoon are most apparent at height but less strongly evident at the surface and then for only several months.

It is possible that the results produced in our simulations could play a critical *triggering* role in ENSO, a role which we would have missed given our experimental setup. Consider the following scenario: The perturbations in the Pacific wind stress field suggested by the T21 model could trigger an equatorial ocean warming that would then force a lower frequency ENSO event in the atmosphere. Although the stress fields differed from the control with high significance in only two months, they appear to have had a low frequency variation, or bias, to which the ocean, acting as an integrator, would be sensitive. Such a signal would escape our significance tests in the presence of high frequency noise. Since SSTs were specified in our snow/monsoon simulations, the T21 model would have no chance to develop a prolonged ENSO event. The above idea was tested the two ways described below.

b. Ocean model experiment

A high resolution, sophisticated model of the equatorial Pacific Ocean (Latif et al. 1985; Latif 1987) was brought to steady state using the annual-cycle stress fields from the observations of Goldenberg and O'Brien (1981). The ocean model was then driven with surface stress anomalies derived from two D experiments beginning 1 January and extending through October. The resulting development of the equatorial Pacific SST field is given in the form of a Hovmöller diagram (Fig. 22, upper). The reader is here cautioned that the fol-

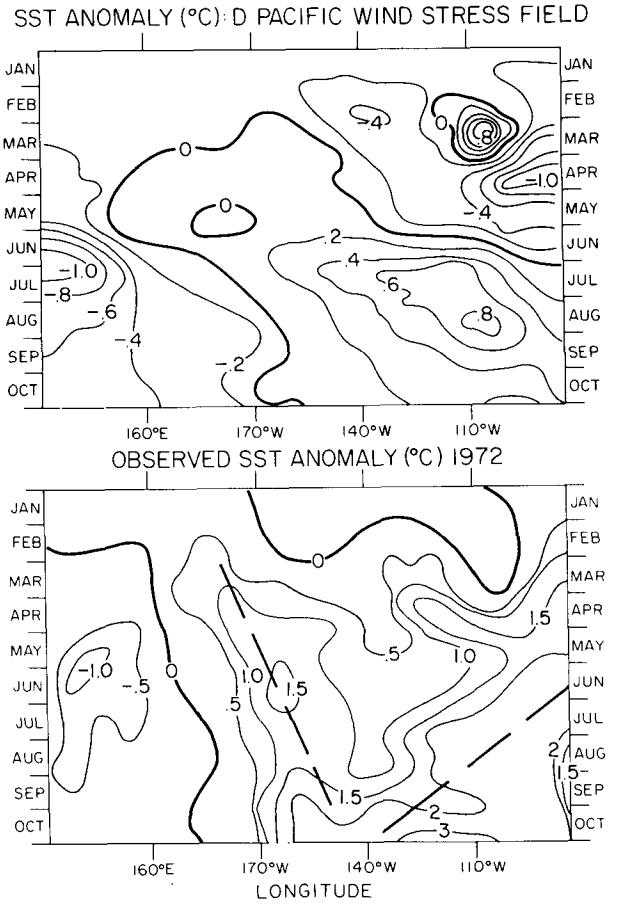

FIG. 22. Upper: Longitude–time diagram showing the evolution of SST anomalies within ±5° of the equator in a model of the tropical Pacific Ocean driven by the average wind stress fields obtained from two D experiments. The ocean model was integrated with wind data beginning 1 January. Anomalies (°C) are relative to values obtained by driving the ocean model with T21 control run wind stresses. Lower: Similar display for SST anomalies (°C) observed in 1972. The dashed lines suggest the sense of zonal displacement of SST anomalies.

lowing results be considered both preliminary and at best qualitative in nature for reasons that will be stated shortly.

The ocean model developed SST anomalies that showed a characteristic eastward propagation. The largest elements of the signal are seen to occur nearly simultaneously with the large May/June stress anomaly in the western Pacific (Rossby wave upwelling) and several months later (the Kelvin wave transit time) in the eastern Pacific. The maximum magnitude of warming in the eastern Pacific peaked briefly at 0.8°C. The short-lived perturbations in that area in March are due to local wind stress anomalies; apparently transients. In summary, the stress field associated with the D experiments produced a mini-El Niño, a result in concert with the empirical studies noted above.

The eastward translation of the SST anomalies shown in Fig. 22 is not characteristic of a "typical" El Niño, (e.g. Barnett 1977; Rasmusson and Carpenter 1982). However, some El Niños do demonstrate this feature to some extent, e.g., the 1972 event (Fig. 22, lower) and 1986 event (Fig. 23, lower), which showed eastward anomaly motion in the western and central Pacific. Clearly the strongest anomaly signal goes westward and that's what has dominated prior analyses. Note 1972 was a poor monsoon year and the positive SST anomalies first appear in both the western Pacific and coast of South America simultaneously in the early spring. If one imagines "classes" of El Niño events each triggered by different physical processes then the above results may belong to one such class. Interestingly, the observed SST anomaly field evolution during other poor monsoon years (not shown) demonstrate features common to Fig. 22 (upper). But they contain large, fundamental differences also.

Based on the above result one might guess that our experimental procedure (specified SST) precluded the simulation of an ENSO event. However, the snow/monsoon perturbation *by itself* is apparently not adequate to sustain a full blown ENSO since:

(i) The D experiment stress anomalies imposed on the ocean model are roughly two times smaller than observations suggest are required for a moderate equatorial warming. It is known however, that the T21 underestimates the observed stress field over the ocean (Fischer 1987).

(ii) The large-scale response of the ocean model is generally small, typically less than 0.5°C over the time and space scales associated with ENSO. Further, the corresponding ocean model sea level responses are also modest with maximum values of 5 cm.

(iii) As noted above, the time scale of the snow/monsoon perturbation is 3–4 months while the ENSO time scale is of order 1–2 yr. Thus, Asian climate anomalies can, at most, trigger ENSO events.

All in all, the snow cover/monsoon signal has all the necessary characteristics to trigger the Pacific portion of an ENSO event—but the signal strength is too small by a factor of at least two, given the original Asian snow cover perturbations used in this study. At least, some of the signal strength weakness is due to shortcomings of the T21 model's simulation of the surface stress field.

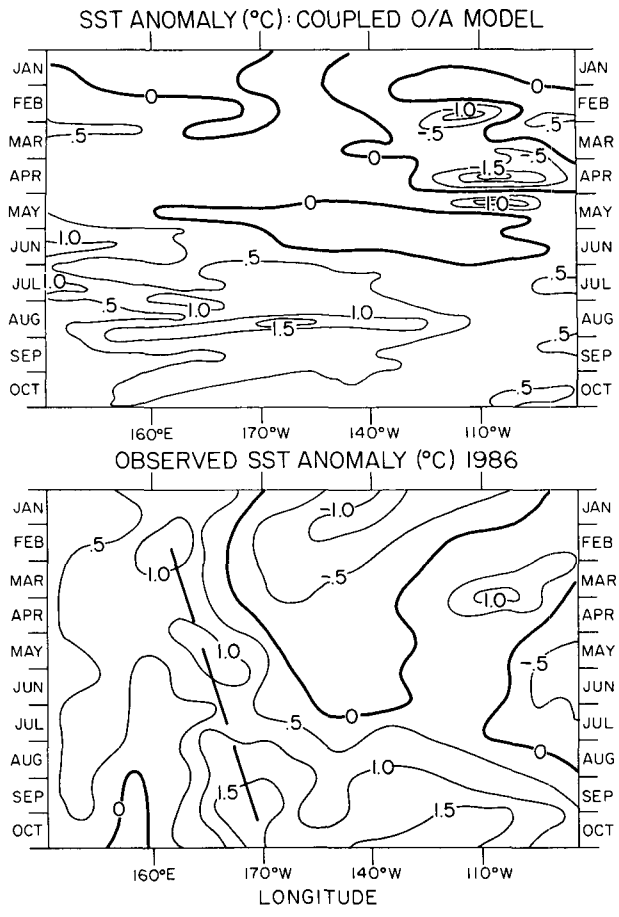

FIG. 23. Upper: As in Fig. 22 but for a coupled ocean–atmosphere model with doubled snowfall over Eurasia as the only perturbation. Note the amplified response of the ocean over that for the uncoupled run (Fig. 22, upper). Lower: As in Fig. 22 but for observed SST anomalies during 1986.

c. *Ocean–atmosphere model experiment*

The T21 atmospheric model next was coupled to the ocean model noted above (Latif et al. 1988) to investigate the effect of perturbations in the snow field on the *coupled* system. A perturbation run with doubled snowfall over Eurasia as the only anomalous forcing was begun on 1 January and continued for one year. The difference between this run and a coupled control run are shown in a Hovmöller diagram for equatorial SST (Fig. 23). Again, the reader is cautioned about the qualitative nature of the results to be discussed below.

Realistic SST anomalies are seen to occur across much of the Pacific several months after the main perturbation in the surface stress field (May–June). Note

the SST feature is now *twice* as strong (1.5°C) as found in the "ocean-only" experiment. The coupled system is clearly amplifying the initial snow-induced perturbation and *that is the key result of this experiment.* The ocean response in the coupled model is not unlike that observed at the start of the 1986–87 El Niño (Fig. 23, lower).

The above results again strongly point to a real snow–monsoon–El Niño connection. But they are not conclusive for the following reasons:

(i) The model El Niño dies out in the late fall, a time when real events reach maximum strength (e.g., Fig. 23, lower). In our experiment, this is due to a strong ocean model drift that results in a substantially cooler SST and the subsequent decoupling of the model ocean from the model atmosphere. This decoupling was evident in the atmospheric model which began to develop SLP anomalies of hemispheric dimension (Southern Oscillation) with an abnormally warm ocean but quickly lost them as the model SST began to cool. Thus, the numerical experiment has serious flaws.

(ii) A monsoon trigger for El Niños dictates a timing on the latter events relative to the annual cycle. Indeed, some warm events off the coast of South America possess the correct seasonal phase to be explained by this mechanism. But some do not. By contrast, warm SST events in the central Pacific always peak in the fall/early winter so their timing relative to the monsoon is correct. Nevertheless, enough variations exist between El Niño events so that the monsoon trigger, if real, can be but one of the "multiple causes" of El Niños.

In summary, the coupled system appears to amplify the initial snow-induced perturbation eventually producing a warming of SST in the model comparable in magnitude to that observed in nature. Initially, the atmospheric model also develops SLP anomalies like those observed. But these die out due to problems in the coupled model. The nature of the model errors is such that their correction should only amplify the positive results obtained during the early stages of the coupled integration. It seems worthwhile to perform and analyze in detail more carefully controlled coupled runs and then to see which historical El Niños might have been associated with a monsoon trigger.

8. Conclusions

We have investigated the long-standing hypothesis that the amount and extent of Asian snow cover has a subsequent effect on the Asian monsoon. Our procedure has been to simulate this idea with a sophisticated atmospheric circulation model. Hence we ran numerous integrations with snowfall rates over Eurasia, both doubled and halved. Comparison with observed variability in Eurasian snow depth and extent suggests these perturbation experiments were realistic. The subsequent regional and remote response were analyzed for statistical significance and compared with observations. Our main findings were:

1) Increased snow cover over Eurasia leads to a subsequent reduction in precipitation over Southeast Asia in the spring and early summer, reduction of wind stress over the Indian Ocean, increased surface pressure over Asia, reduced land and tropospheric temperatures, and other elements associated with a "poor" monsoon. Decreased snow cover over Eurasia produces just the opposite results. In essence, the model simulations support the hypothesized snow–monsoon relationship and agree with observations. Thus, the numerical results substantiate an hypothesis offered over 100 years ago (Blanford 1884) plus support one key element in the observed sequential variation of low frequency global climate fluctuation offered more recently by Barnett (1985a).

2) The physical processes responsible for the regional response are complex and act in two stages. With snow present on the ground albedo, evaporative fluxes and the heat of fusion (needed to melt the snow) dominate the energy budget. Once the snow has melted evaporative fluxes, albedo changes due to atmospheric water vapor (clouds) and the physics of the soil hydrology become important. It is processes associated with the latter cycle that provide a "memory" for the regional climate system after all the snow has melted. In either stage, the net result of these processes is to alter the land–ocean temperature contrast needed to initiate the monsoon and thus affect its strength.

3) Large-scale remote responses induced by the snow cover/monsoon perturbation exist between Asia and North America, and Asia and the equatorial zone. The former response takes the form of a dipole in the SLP field with poles over Asia and the oceans surrounding North America. This response, which takes the form of a baroclinic wave ($k = 1$), is due to anomalous thermal forcing associated with enhancement of the land–sea temperature contrast. Observations marginally support the existence of this model response. The equatorial response was more or less zonally uniform and resulted from large-scale snow-related precipitation (latent heat release) anomalies over Southeast Asia. This response was also found in the control simulations and so was a natural mode of variation in the numerical model. In this case, the response was due to large-scale, stochastic variation in the precipitation field of the IndoPacific region. This large-scale remote response is found also in observed data.

4) Remote, near-surface responses in the atmosphere over the equatorial Pacific were found in the surface wind and heat flux fields. The wind stress anomalies, when used to force an ocean model, produced a weak El Niño under prior conditions of heavy Eurasian snowfall and poor monsoon. This sequence of events resembled those observed during ENSO events. However, the snow cover/monsoon trigger appears too weak to force, by itself, a large-scale equatorial warming of the magnitude observed. The snowfall perturbation experiment when carried out with a coupled ocean–atmosphere model produced a fairly realistic El

Niño twice the size of that found in the "ocean model only" experiment. The coupled system clearly seems capable of amplifying the initial snow-induced perturbation. While many of the features of the model-generated El Niños appear realistic, there are also substantial dissimilarities with observations plus problems with the simulations themselves. In balance, it appears that snow-induced monsoon perturbations may be one of the (multiple) triggers that can initiate an ENSO cycle. Thus, it appears that land surface processes over Eurasia play a vital role in the climate variations of that region and may also be important to global climate variations, e.g., ENSO events.

We wish to conclude by reminding the reader of the more serious shortcomings of this paper:

1) The model resolution is too coarse to allow detailed simulation of the various regional monsoons over Southeast Asia. Rather, our results apply to the Asian monsoon in the most macroscopic sense. It thus seems worth repeating the experiments reported here with a higher resolution model so the role of snow in the regional monsoon can be investigated.

2) The perturbation snowfall for the D and H experiments about the control mean seems fairly realistic with regard to depth but we are less certain about the zonal extent of the anomaly. Further, one should remember that the model mean does represent a larger than observed snow cover, particularly in June. This means that the "snow physics" may, on average in our simulations, play an exaggerated role in forcing the atmosphere. However, the H experiments produce snow cover that is close to or less than the observed climatology. Since the H–C experimental results are highly significant, we expected our results to be reasonable subject to the proviso regarding snow extent.

3) The ocean and coupled ocean–atmosphere model results discussed in section 7 should be thought of as preliminary. However, all of the results suggest the strong likelihood of a snow–monsoon–El Niño connection and for that reason, plus the empirical support for such a relation, we have included them in this paper. We further feel that the problems with the simulations are such as to *understate* the degree of coupling in the triple interaction noted above. Elimination of major model errors will almost surely enhance the feedback already documented in section 7.

Acknowledgments. This work was supported by Climate Dynamics Program of NSF through Grant ATM85-13713. Support was also given by Deutsche Forschungsgemeinschaft through SFB 318 and by Bundesminister für Forschung und Technologie, Grant K-F 20128. The authors would also like to express their appreciation to the Max-Planck-Institut für Meteorologie, Hamburg, for additional support of this work. Shy Chen, Isaac Held, Nick Graham and particularly John Roads provided useful suggestions during the preparation of this manuscript as well as being good sounding boards. Tony Tubbs patiently carried through the voluminous graphic calculations associated with this study. Mike Matson kindly provided an updated, corrected version of the Asian snowcover dataset on short notice. Jay Winston generously shared his radiation data for comparison with the model results. M. Zimmerman and L. Foster of ETAC kindly provided the observed snow data and that data played a critical role in ascertaining the realism of the snow cover perturbation developed in the model.

REFERENCES

Angell, J. K., 1981: Comparison of variations in atmospheric quantities with sea surface temperature variations in the equatorial eastern Pacific. *Mon. Wea. Rev.*, **109**, 230–243.

Barnett, T. P., 1977: An attempt to verify some theories of El Niño. *J. Phys. Oceanogr.*, **7**, 633–647.

——, 1985a: Variations in near-global sea level pressure. *J. Atmos. Sci.*, **42**, 478–501.

——, 1985b: Three-dimensional structure of low frequency pressure variations in the tropical atmosphere. *J. Atmos. Sci.*, **42**, 2798–2803.

Bilello, M., 1984: Regional and seasonal variations in snow cover density in the USSR. CR-REL, Rep. 84–22, PP15, [available from U.S. Army Corps of Engineers, Cold Regions Research and Engineering Laboratory, Hanover, New Hampshire.]

Blanford, H. F., 1884: On the connexion of Himalayan snowfall and seasons of drought in India. *Proc. Roy. Soc. London*, **37**, 3–22.

Chervin, R., and S. Schneider, 1976: On determining the statistical significance of climate experiments with general circulation models. *J. Atmos. Sci.*, **33**, 405–412.

Cornejo-Garrido, A. G., and P. Stone, 1977: On the heat balance of the Walker circulation. *J. Atmos. Sci.*, **34**, 1155–1162.

Dey, B., and O. S. R. U. Bhanu Kumar, 1982: An apparent relationship between Eurasian snow cover and the advanced period of the Indian summer monsoon. *J. Appl. Meteor.*, **21**, 1929–1932.

——, and ——, 1983: Himalayan winter snow cover area and summer monsoon rainfall over India. *J. Geophys. Res.*, **88**, 5471–5474.

Dickson, R. R., 1984: Eurasian snow cover versus Indian monsoon rainfall—An extension of the Hahn-Shukla results. *J. Climate Appl. Meteor.*, **23**, 171–173.

Elliott, W., and J. Angel, 1987: The relation between the Indian monsoon rainfall, the Southern Oscillation, and hemispheric air and sea temperature: 1884–1984. *J. Climate Appl. Meteor.*, **26**, 943–948.

Fein, J., and P. Stevens, 1987: *Monsoons*, Wiley and Sons, 632 pp.

Fischer, G. (Ed.), 1987: Large-scale Atmospheric Modelling. Rep. No. 1, Meteor. Inst. University Hamburg.

Flohn, H., 1957: large-scale aspects of the "summer monsoon" in south and east Asia. *J. Meteor. Soc. Jpn.*, (75th annual volume), 180–186.

Goldenberg, S., and J. O'Brien, 1981: Time and space variability of the tropical Pacific wind stress. *Mon. Wea. Rev.*, **109**, 1190–1207.

Graham, N. E., T. P. Barnett, R. M. Chervin, M. E. Schlesinger and U. Schlese, 1988: Comparisons of GCM and observed surface wind fields over the tropical Indian and Pacific Oceans. *J. Atmos. Sci.*, in press.

Hahn, D. J., and J. Shukla, 1976: An apparent relationship between Eurasian snow cover and Indian monsoon rainfall. *J. Atmos. Sci.*, **33**, 2461–2462.

Hastenrath, S., 1985: *Climate and Circulation of the Tropics*. D. Reidel, pp. 455.

He, H., J. McGinnis, Z. Song and M. Yanai, 1987: On the onset of Asian summer monsoon in 1979 and the effect of the Tibetan plateau. *Mon. Wea. Rev.*, **115**, 1966–1995.

Held, I. M., 1983: Stationary and quasi-stationary eddies in the extratropical troposphere: Theory. *Large-scale Dynamical Processes in the Atmosphere,* B. Hoskins and R. Pearce, Eds., Academic Press, 127–170.

Horel, J., and J. Wallace, 1981: Planetary scale atmospheric phenomena associated with the Southern Oscillation. *Mon. Wea. Rev.,* **109,** 813–829.

Jaeger, L., 1976: Monatskarten des Niederschlags für die ganze Erde. *Ber. Dtsch. Wetterdienstes,* **18,** (139), 38 pp.

Johnson, D., R. Townsend and M.-Y. Wei, 1985: The thermally coupled response of the planetary scale circulation to the global distribution of heat sources and sinks. *Tellus,* **37a,** 106–125.

Khandekar, M. L., and V. R. Neralla, 1984: On the relationship between the sea surface temperatures in the equatorial Pacific and the Indian monsoon rainfall. *Geophys. Res. Lett.,* **11,** 1137–1140.

Kopanev, I. D., and V. I. Lipovaskaya, 1978: Distribution of snow depth in the U.S.S.R. *Trudy,* **361,** 72–86. CRREL Bibliography Accessioning No. 32–616.

Krishnamurti, T. M., 1971: Tropical east–west circulations during the northern summer. *J. Atmos. Sci.,* **28,** 1342–1347.

Kukla, G., and D. Robinson, 1981: Climatic value of operational snow and ice charts. Glaciological Data Rep. *GD–11,* World Data Center A for Glaciology, Boulder, CO, 103–119, (NTIS No. PP82 169301).

Kuo, H. L., 1974: Further studies of the parameterization of the influence of cumulus convection on large-scale flow. *J. Atmos. Sci.,* **31,** 1232–1240.

Kutzbach, J., 1981: Monsoon climate of the early Holocene: Climate experiment with the earth's orbital parameters for 9000 years ago. *Science,* **214,** 59–61.

Latif, M., 1987: Tropical ocean circulation experiments. *J. Phys. Oceanogr.,* **17**(2), 246–263.

——, E. Maier-Reimer and D. J. Olbers, 1985: Climate variability studies with a primitive equation model of the equatorial Pacific. *Coupled Ocean-Atmosphere Models,* J. C. J. Nihoul, Ed., Elsevier Science Publishers.

——, J. Biercamp and H. von Storch, 1988: The response of a coupled ocean–atmosphere general circulation model to wind bursts. *J. Atmos. Sci.,* **45,** 964–979.

Lau, K.-M., and M.-T. Li, 1984: The monsoon of East Asia and its global association—A survey. *Bull. Amer. Meteor. Soc.,* **65,** 114–125.

Livezey, R., and W. Chen, 1983: Statistical field significance and its determination by Monte Carlo techniques. *Mon. Wea. Rev.,* **111,** 46–59.

Matson, M., and D. Wiesnet, 1981: New data base for climate studies. *Nature,* **288,** 451–456.

Meehl, G. A., and W. M. Washington, 1988: A comparison of soil moisture sensitivity in two global climate models. *Mon. Wea. Rev.,* **45,** 1476–1492.

Mooley, D., and B. Parthasarathy, 1983: Variability of the Indian summer monsoon and tropical circulation features. *Mon. Wea. Rev.,* **111,** 967–978.

——, —— and G. B. Pant, 1986: Relationship between Indian summer monsoon rainfall and location of the ridge at the 500-mb level along 75°E. *J. Climate Appl. Meteor.,* **25,** 633–640.

Namias, J., 1962: Influences above normal surface heat sources and sink on atmospheric behavior. *Proc. of the Int. Symp. of Numerical Weather Prediction,* 615–629. Meteorological Society of Japan, Tokyo. [Available via Japanese Meteorological Agency, 1–3–4 Ote-Machi, Chyoda-Ku, Tokyo.]

——, 1985: Some empirical evidence for the influence of snow cover on temperature and precipitation. *Mon. Wea. Rev.,* **113,** 1542–1553.

Parthasarathy, B., and D. A. Mooley, 1978: Some features of a long homogeneous series of Indian summer monsoon rainfall. *Mon. Wea. Rev.,* **106,** 771–781.

Preisendorfer, R., and T. P. Barnett, 1983: Numerical model-reality intercomparison tests using small-sample statistics. *J. Atmos. Sci.,* **40,** 1884–1896.

Pupkov, V. N., 1964: Formation, distribution, and variation of snow cover on the Asiatic territory of the U.S.S.R. *Meteorology and Hydrology,* **8,** Tp–34–40.

Ramage, C. S., 1971: *Monsoon Meteorology,* Academic Press, 277 pp.

Rasmusson, E., and T. Carpenter, 1982: Variations in tropical sea surface temperature and surface winds associated with the Southern Oscillation/El Niño. *Mon. Wea. Rev.,* **110,** 354–384.

——, and ——, 1983: The relationship between eastern equatorial sea surface temperatures and rainfall over India and Sri Lanka. *Mon. Wea. Rev.,* **111,** 517–527.

Rikhter, G. D., 1954: Snow cover, its formation and properties. Izdatel'Stvo Akademiia Nauk SSSR, Moscow, 120 pp., U.S. Army Snow, Ice, and Permafrost Research Establishment (SIPRE), translation no. 6, AD 0459501.

Roads, J. O., 1980: Climate-anomaly experiments in middle latitudes. *Tellus,* **32,** 410–427.

——, 1981: Linear and nonlinear aspects of snow albedo feedbacks in atmospheric models. *J. Geophys. Res.,* **86,** 7411–7424.

Robock, A., 1983: Ice and snow feedbacks and the latitudinal and seasonal distribution of climate sensitivity. *J. Atmos. Sci.,* **40,** 986–997.

Ropelewski, C., A. Robock and M. Matson, 1984: Comments on "An apparent relationship between Eurasian spring snow cover and the advanced period of the summer monsoon." *J. Climate Appl. Meteor.,* **23,** 341–342.

Schutz, C., and L. B. Bregman, 1987: Global annual snow accumulation by months. RAND Note N-2551-AS, [available from Rand Corporation, 1700 Main St., Santa Monica, CA 90406.]

Shukla, J., and J. M. Wallace, 1983: Numerical simulation of the atmospheric response to equatorial Pacific sea surface temperature anomalies. *J. Atmos. Sci.,* **40,** 1613–1630.

Simmons, A. J., and R. Burridge, 1981: A energy and angular-momentum considering finite difference scheme, hybrid coordinates, and medium-range weather prediction. ECMWF Tech. Rep. No. 28, 68 pp.

Smagorinsky, J., 1953: The dynamical influence of large-scale heat sources and sinks on the quasi-stationary mean motions of the atmosphere. *Quart. J. Roy. Meteor. Soc.,* **79,** 342–366.

Tanaka, N., 1980: Role of the circulation of 150 mb level in the winter in summmer monsoon in the Asian and Australian regions. *Climatol. Notes,* **26,** Institute of Geoscience, University of Tsukuba.

von Storch, Hans, T. Bruns, I. Fischer-Bruns and K. Hasselmann, 1988: Principal oscillator pattern analysis of the 30–60 day oscillation in a GCM equatorial troposphere. Max-Planck-Institut für Meteorologie, Rep. No. 7.

Walker, G. T., 1910: On the meteorological evidence for supposed changes of climate in India. *Mem. Indian Meteor.,* **21,** 1–21.

Wallace, J. M., S. Tibaldi and A. J. Simmons, 1983: Reduction of systematic forecast errors in the ECMWF model through the interaction of an envelope orography. *Quart. J. Roy. Meteor. Soc.,* **109,** 683–717.

Walsh, J., W. Jespersen and D. Ross, 1985: Influences of snow cover and soil moisture on monthly air temperature. *Mon. Wea. Rev.,* **113,** 756–768.

Weare, B., 1979: Statistical study of the relationship between ocean surface temperatures and the Indian monsoon. *J. Atmos. Sci.,* **36,** 2279–2291.

Webster, P., L. Chou and K.-M. Lau, 1977: Mechanisms effecting the state, evolution, and transition of the planetary scale monsoon. *Pure Appl. Geophys.,* **115,** 1463–1490.

Wei, M.-Y., A. Johnson and R. Townsend, 1983: Seasonal distributions of diabatic heating during the first GARP global experiment. *Tellus,* **35a,** 241–255.

Wu, M.-C., and S. Hastenrath, 1986: On the interannual variability of the Indian monsoon and the Southern Oscillation. *Arch. Meteor. Geophys. Bioklim.,* **B36,** 239–261.

Yasunnari, T., 1987: Global structure of the El Niño/Southern Oscillation, Part II: Time evolution. *J. Meteor. Soc. Jpn.,* **65,** 81–102.

Yeh, T.-C., R. Wetherald and S. Manabe, 1983: A model study of the short term climatic and hydrological effects of sub-snow cover removal. *Mon. Wea. Rev.,* **111,** 1013–1024.